SEDIMENTOLOGY the journal of the International Association of Sedimentologists IAS

Sedimentology (2026) **73**, 40–82 doi: 10.1111/sed.70048

Facies mosaic distribution and stratigraphic disorder of a mixed carbonate–siliciclastic tidal succession

VICTOR J. P. HÊME DE LACOTTE*, CHESTER H. C. DAVIES*, BRIONY J. BOWLER*, STUART M. CLARKE*, A. GRAHAM LESLIE*,† and DOUGLAS A. SPRINKEL‡

**Basin Dynamics Research Group, School of Life Sciences, Keele University, Keele ST5 5BG, UK (E-mail: v.j.p.heme.de.lacotte@keele.ac.uk)*

†British Geological Survey, The Lyell Centre, Research Avenue South, Edinburgh EH14 4AP, UK

‡Azteca Geosolutions, Pleasant View, UT 84414, USA

Associate Editor – Marc Aurell

ABSTRACT

Complex stratigraphic arrangements may be generated through lateral facies transitions from the strata of aeolian depositional systems into bordering peritidal deposits. In such scenarios, sedimentary architectural complexity and associated facies heterogeneities are governed by the interplay between autogenic processes inherent to tidal environments and larger-scale allocyclic forcing. As a result, complications arise when trying to discriminate the two signals within preserved strata, and the prediction of their depositional configuration may be challenging. By documenting the facies diversity and spatial distribution of an ancient mixed carbonate–siliciclastic tidal flat succession deposited under arid conditions, and by analysing its degree of stratal disorder, this work provides a generalised model for the stratigraphic record of marginal mixed peritidal flats. The sedimentology of tidally dominated shallow marine to sabkha deposits of the Middle Jurassic Carmel Formation (San Rafael Group) is investigated across a 350 km long transect in southern Utah, USA. A total of 26 lithofacies are identified and grouped into 11 facies associations. Detailed qualitative and quantitative analysis of facies distribution has highlighted two transgressive-regressive sequences overprinted by high levels of autogenic noise at the facies association scale. Multiple coexisting associations are observed within different facies belts and are characterised by the sedimentary signatures of intricate coastal, tidal and aeolian forces with variable proportions of carbonate, siliciclastic and evaporitic material. By combining statistical analysis with classical sedimentological interpretations, this study demonstrates the challenges in predicting the distribution of discrete stratigraphic architectures in peritidal successions. Such systems may be subdivided into separate depositional elements defined by differences in facies proportions linked to changes in depositional processes and energy levels across their margins. This work proposes a newly quantified model for arid tidal systems with which to account for stratal disorder. Incorporating this singular characteristic may help constrain the predictions of reservoir heterogeneities in analogous subsurface successions.

Keywords autocyclic, Carmel Formation, depositional model, facies mosaic, mixed carbonate–siliciclastic, Tidal.

INTRODUCTION

Tidally dominated, carbonate-rich marine margins to arid continental systems are the scene of complex interactions between multiple sedimentary processes which together give rise to some of the most challenging stratigraphic records to interpret. Whilst sedimentary successions of aeolian systems are generally fairly prone to recording the influence of allocyclic controls and thus to expressing sedimentary cyclicity in their stratigraphic record, marginal paralic systems may be influenced by a combination of auto-and allogenic processes that together make their analysis in the rock record challenging.

Sedimentary heterogeneities in tidally dominated successions are observed at every scale (Yoshida *et al.*, 2001; Ainsworth, 2010; Chiarella *et al.*, 2017, 2024) and relate to a wide range of autogenic mechanisms (e.g. Pratt & James, 1986; Cloyd *et al.*, 1990; Osleger, 1991; Musial *et al.*, 2012; Olariu *et al.*, 2012; Longhitano & Miocic, 2024) and allogenic forces (e.g. Yoshida *et al.*, 2007; Longhitano & Miocic, 2024; Wroblewski *et al.*, 2024). Interactions between wave, tide and aeolian processes, coupled with the mixing of different sediment types (i.e. siliciclastic, carbonates, evaporites), can result in the preservation of high lithofacies diversity and highly varied vertical trends. Nevertheless, interpretations of apparent peritidal stratigraphic sequences based on the preconceived notion that canonical shallowing upward cycles (James, 1984) are solely the product of sea-level change are still common practice for most outcrop-based studies (e.g. Spalluto *et al.*, 2024). The foundational theory on the role of eustasy in recorded carbonate cyclicity (Demicco, 1985; Grotzinger, 1986; Koerschner & Read, 1989; Goldhammer *et al.*, 1990) is a powerful tool to interpret broad-scale stratigraphic sequences, but it cannot explain all facies transitions observable at a detailed level (Rivers & Dalrymple, 2025). Pioneering work from Wilkinson *et al.* (1996, 1997) and, more recently, forward-modelling methods introduced by Burgess (2006, 2016) suggest that observed patterns in peritidal carbonate successions may be only perceptional artefacts, and that sequence analysis should be statistically supported as well as interpretatively examined. Nevertheless, the effects of scattered facies distribution (i.e. facies mosaic) in tidal flats and their inherited stratigraphic disorder are only rarely discussed (Manifold *et al.*, 2020; Quijada *et al.*, 2020; Geyman *et al.*, 2021).

Sediments of aeolian systems make demonstrably good regional-scale reservoirs for carbon capture and storage, and bordering tidal sediments along their margins have the potential to provide excellent regional-scale stratigraphic seals. However, current models for mixed peritidal flats do not fully account for the architectural complexity arising from the randomised mosaic distribution of facies at the time of deposition. Documenting the inter-dependence of such depositional environments through geological time and unravelling the combination of controls that drives their stratigraphic heterogeneities is therefore crucial for targeting aeolian sandstone deep saline aquifers for CO_2 sequestration (e.g. Priddy *et al.*, 2023).

This work discusses the sedimentology of a mixed carbonate and siliciclastic arid tidal flat succession and presents a generic facies model that accounts for preserved heterogeneities and stratigraphic architectures arising from plan-view facies mosaic distributions. The study shows an analysis of the spatio-temporal evolution of the Carmel Formation: a Bajocian shallow-marine succession deposited along the shoreline of an epicratonic seaway flooding the Colorado Plateau of the western USA. Specific objectives are: (i) to evaluate the facies diversity and relationships to stratigraphic complexity for mixed carbonate–siliciclastic arid tidal flats; (ii) to discuss the vertical stratal disorder that is characteristic of tidal successions; (iii) to investigate the influence of plan-view facies mosaic distribution on apparent stratigraphic disorder through comparison with a modern example. Aeolian deposits of the contemporaneous Page Sandstone are discussed where they occur in association with tidal deposits, but their comprehensive analysis is beyond the scope of this study.

BACKGROUND

Interplay between tidal, wave and fluvial processes in coastal environments leads to a broad spectrum of depositional products with differing relative sedimentary characteristics associated with each driving force (Galloway, 1975; Dalrymple *et al.*, 1992; Ainsworth *et al.*, 2011; Vakarelov *et al.*, 2012; Zuchuat *et al.*, 2023). Furthermore, it is now recognised that basin geometry (Zuchuat *et al.*, 2022) and

palaeocoastline morphology (Sleveland *et al.*, 2020) can control, or at least influence significantly, the preserved stratigraphic record of tidal cyclicity. Consequently, confined tidal systems within restricted basins (e.g. epicontinental seaways) will tend to be the scene of complex overprints from autogenic signals, such as tidal amplification processes (Zuchuat *et al.*, 2019) or sediment reworking during storm events (Kvale *et al.*, 1995), which may make the recognition of allogenic cycles recorded in strata challenging. To compound the complexity, the record of tidal signature, when present, can be observed at different wavelengths preferentially expressed in particular depositional settings (Tessier & Gigot, 1989; Longhitano, 2011; Longhitano *et al.*, 2012b).

Further challenges arise when trying to link depositional processes to the stratigraphic record of mixed carbonate–siliciclastic tidal systems. In such scenarios, multi-scale interactions may involve terrigenous siliciclastic content and locally produced biogenic material or bioclastic material derived from a nearby carbonate factory. Such complex tidal systems are well recognised in the rock record. Some studies document sedimentary processes which decouple deposition of externally sourced siliciclastic detritus (e.g. fluvial sediment pulses) from localised carbonate deposition (Breda & Preto, 2011; Quijada *et al.*, 2016; Wroblewski & Schueth, 2023), whilst others illustrate scenarios of coeval mixing between the same two sediment fractions (Longhitano *et al.*, 2012b; Chiarella *et al.*, 2017; Bádenas *et al.*, 2018). At the bed scale, heterolithic segregation of quartz and bioclastic grains stems from the laws of hydrodynamics (Chiarella & Longhitano, 2012) and tidal modulation (Longhitano *et al.*, 2010; Longhitano, 2011). When upscaled to stratigraphic scale, intertongued, vertically stacked patterns of carbonate and siliciclastic packages are more likely to be driven by transgressive-regressive relative sea-level cycles linked to eustatic variations (e.g. Spalluto, 2008), salt tectonics (e.g. Bourillot *et al.*, 2010) or structural dynamics (e.g. Wroblewski & Morris, 2023).

For mixed tidal flats in hot desert climates where arid conditions prevail (20° to 30° latitudes ranges; Peel *et al.*, 2007), sub- to intertidal microbial activity, the formation of ooidal barrier islands and supratidal evaporitic precipitation (i.e. sabkha) are often the main driving mechanisms for in situ carbonate grain production, while siliciclastic material is derived mainly from ephemeral wadi-type river systems that reach the coastal plains (Breda & Preto, 2011), or from bordering aeolian ergs (Fryberger *et al.*, 1990; Rodríguez-López *et al.*, 2012; Cross *et al.*, 2023). Multi-scale studies documenting Holocene evolution of low-gradient carbonate ramps and sabkhas along the southern Arabian Gulf coastline have produced well-constrained geomorphological models for modern arid peritidal environments (Lokier & Steuber, 2008; Lokier *et al.*, 2013; Lokier & Fiorini, 2016; Rivers *et al.*, 2020). Dedicated summaries of sedimentary processes and classification of sub-environments found in such settings are numerous (e.g. Alsharhan & Kendall, 2003; Pratt, 2010; Lasemi *et al.*, 2012). However, prevailing geological models used for associated subsurface interpretations don't account for preserved heterogeneities and architectural complexities, despite active applied research on reservoir characterisation in such depositional systems (e.g. Grötsch *et al.*, 2003; Longhitano *et al.*, 2012a; Qiao *et al.*, 2016; Khazaie *et al.*, 2022). By investigating the lithofacies diversity and spatiotemporal distribution of an ancient arid mixed tidal succession, this study proposes a generalised model for such systems with which to account for recorded stratal signatures of competing autocyclic and allocyclic controls.

GEOLOGICAL SETTING

From late Palaeozoic through to Jurassic times, the stratigraphic record of the Colorado Plateau in the western USA is dominated by deposits associated with arid climates (Blakey *et al.*, 1988; Parrish & Peterson, 1988). From southern Wyoming to northern Arizona, most of the Middle Jurassic strata are characterised by widespread erg successions interacting with shallow-marine deposits from the Sundance Seaway (Fig. 1E). These deposits filled a retro arc foreland basin – the Utah-Idaho Trough – as the region drifted northward into the intertropical convergence zone (Kocurek & Dott, 1983; Danise & Holland, 2017). This depocentre has been linked to Jurassic Cordilleran tectonics and is the result of an asymmetric flexural subsidence in the foreland of the Elko Orogenic Belt (Bjerrum & Dorsey, 1995; Kowallis *et al.*, 2001; Thorman, 2011). It is bound to the east by several palaeo-highs including remnant topographies of the Uncompahgre, Defiance and Monument

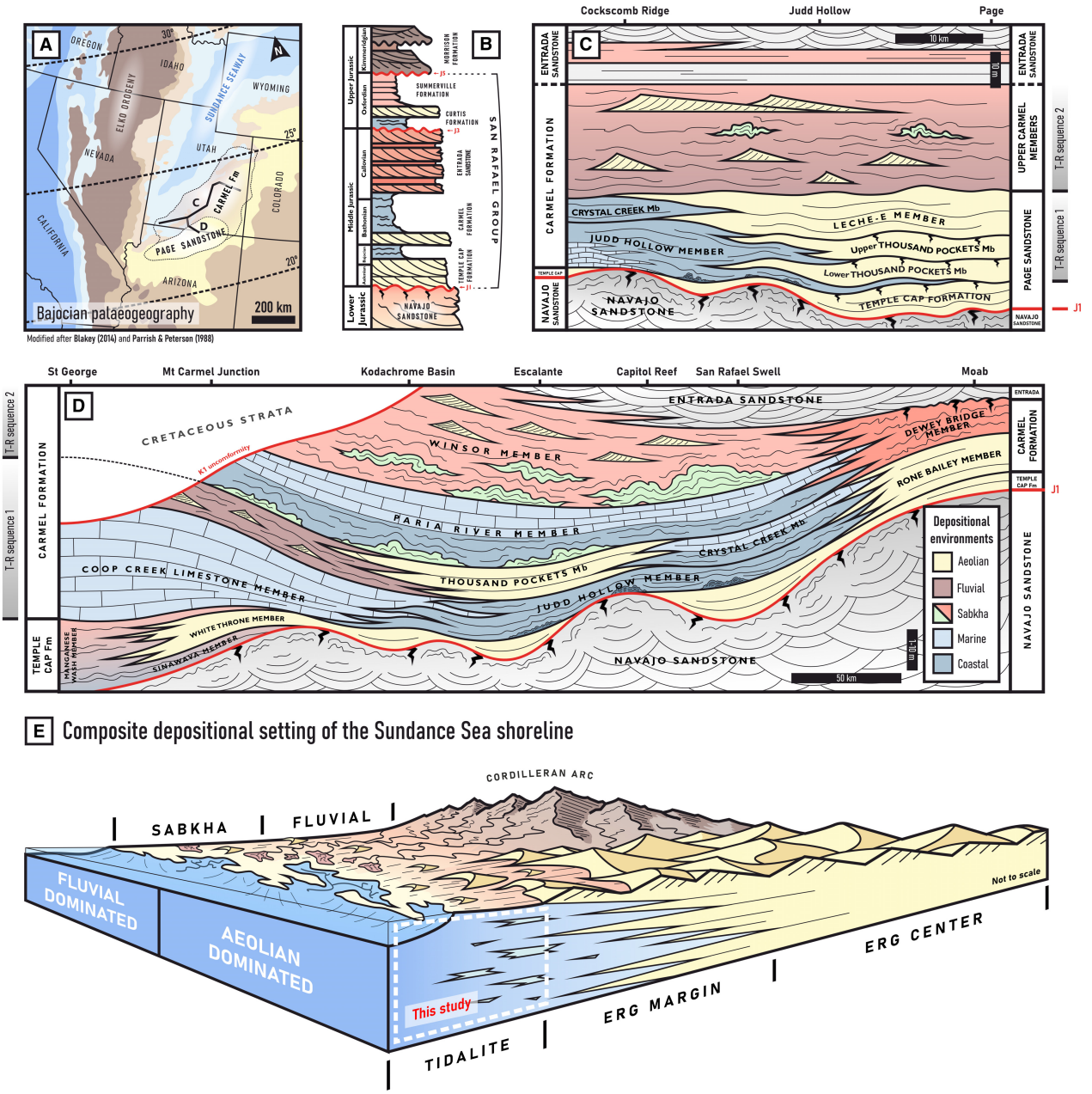

Fig. 1. (A) Bajocian palaeogeographical setting of the Colorado Plateau displaying the extents of the Sundance Sea incursion and the coastal Page erg. Adapted from Blakey (2014) and Parrish & Peterson (1988). (B) Simplified stratigraphic log of the San Rafael Group in southeastern Utah. (C, D) Lithostratigraphic framework for the Carmel Formation, the Page Sandstone and the Temple Cap Formation on transects perpendicular (C) and parallel (D) to the Sundance Sea palaeocoastline. The Carmel Formation is subdivided into eight lithostratigraphic members whose definitions are based upon transgressive-regressive trends and lateral facies changes. (E) Composite model of the Sundance Sea summarising the various depositional environments observable in the different deposits of the San Rafael Group. Theoretical position of this work's focus is given.

uplifts as well as the Ancestral Uinta Arch (Blakey *et al.*, 1988; Sprinkel *et al.*, 2024), whereas its southern border gradually grades into the Mogollon Slope, an exhumed continental paleo-drainage located in modern Arizona (Bilodeau, 1986). The Utah-Idaho Trough deepens

further north and is thought to have been connected with the Pacific Ocean in modern-day Yukon (Blakey, 2014).

The Bajocian to Callovian (169–162 Ma) Carmel Formation belongs to the San Rafael Group (Fig. 1B) in southeastern Utah, and is attributed to the first major flooding event of the restricted epicratonic Sundance Seaway along the north–south axis of the Utah-Idaho Trough (Fig. 1A). The Formation comprises a mix of shallow-marine carbonates, tidal clastics and coastal sabkha sediments that fit within a complex lithostratigraphic framework of contemporaneous strata (Gilbert, 1877; Gilluly, 1929; Peterson & Pipiringos, 1979; Blakey *et al.*, 1983). It is characterised by two main transgressive-regressive (T-R) sequences (*sensus* Embry & Johannessen, 1993; Fig. 1C and D), the lower of which conformably overlies the marginal aeolian deposits of the Temple Cap Formation (Dickinson *et al.*, 2010; Doelling *et al.*, 2013) and was previously separated from them by the now obsolete J-2 unconformity (Pipiringos & O'Sullivan, 1978; Lucas & Anderson, 1997).

A complex subdivision of the Carmel Formation based upon transgressive-regressive trends has resulted in eight lithostratigraphic members (Fig. 1C and D), some of which are identified as lateral lithological variations of the same depositional sequence (Sprinkel *et al.*, 2011, 2024; Doelling *et al.*, 2013). The reddish tidal flat sandstones and siltstones of the Judd Hollow Member and the alternating thick carbonates and marls of the Co-op Creek Member represent the transgressive system tract (TST) of the first T-R sequence of the Carmel Formation. The overlying large aeolian cross-bedded sandstone sets of the Thousand Pockets Member, and the fine reddish tidal siltstones and evaporitic gypsum beds of the Crystal Creek Member, are associated with the regressive system tract (RST) of this sequence. Both the Co-op Creek and Crystal Creek members illustrate basinward facies transitions to sediment of deeper marine depositional systems. The transgressive event that marks the onset of the second T-R sequence is represented by sediments of the Paria River Member. These sediments range from shallow-marine carbonate sediments in the San Rafael Swell area of Utah, to an ephemeral-fluvial succession in the Vermillion Cliffs area. Specific attention has been given to the Paria River Member in this latter region as this continental part of the Carmel Formation exposes the unusual sedimentology of aeolian-fluvial interactions (Jones & Blakey, 1997) and catastrophic debris flow deposits sourced from the western magmatic arc (Chapman, 1989; Kowallis *et al.*, 2020) as well as intriguing post-depositional deformation features (Wheatley & Chan, 2018). The RST of the second T-R sequence is defined by the Winsor Member that comprises a cyclic coastal sabkha succession of banded siltstones and mudstones intercalated with evaporitic gypsum beds. Southward, sediments of the Carmel Formation intertongue with the dry aeolian deposits of the Page Sandstone south of Page, Arizona (Jones & Blakey, 1993; Blakey *et al.*, 1996; Anderson *et al.*, 2024). Westward, they grade into the mixed offshore sediments of the Arapien Formation (Picard & Uygur, 1982) and northward into the carbonate deposits of the Twin Creek Limestone (Sprinkel, 1982). Sediments of the Carmel Formation grade conformably vertically into the wet aeolian successions of the overlying Entrada Sandstone (Kocurek, 1981a; Crabaugh & Kocurek, 1993). Ichnological and sedimentological analysis of shallow-marine parts of this system suggest together that generally hypersaline and stressed conditions prevailed during the sedimentation of the Carmel Formation (De Gibert & Ekdale, 1999, 2002).

METHODOLOGY

A set of 26 sedimentary logs has been compiled across the extensive outcrop belt of the sediments of the Carmel Formation and the underlying Temple Cap Formation in Utah. Eleven logs have been measured along a 300 km long northeast–southwest basinward transect from Uneva Mine Canyon on the eastern reef of the San Rafael Swell (Section 1, Fig. 2) to Cedar Ridge near Saint George (Section 12, Fig. 2).

Fig. 2. Outcrop distribution map of the Middle Jurassic San Rafael Group and stratigraphically equivalent units with location of studied sections. The proposed stratigraphic framework in Fig. 14 includes Sections 1 to 12. Markov chain analysis covers sedimentary logs from Sections 1 to 3. Geological mapping data is extracted from Hintze *et al.* (2000).

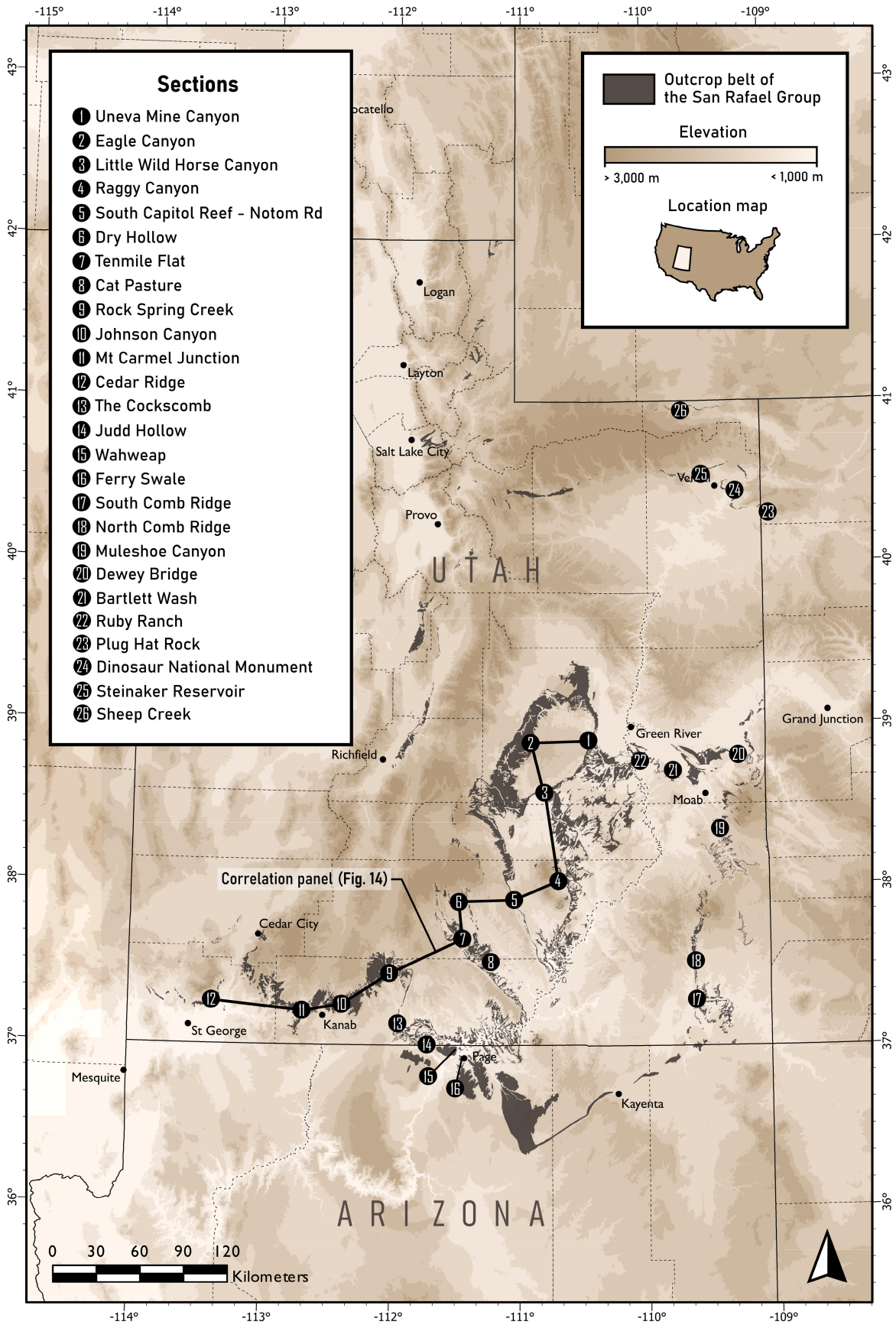

Additionally, 15 logs were collected in equivalent continental parts of the depositional system including (i) the fluvially dominated Bluff and Moab sections (Sections 17 to 21, Fig. 2); (ii) the aeolian dominated Page Sandstone near the northern Arizona state line (Sections 13 to 16, Fig. 2) and (iii) sabkha dominated regions north and south of the Uinta Mountains (Sections 23 to 26, Fig. 2). Each section has been logged at a decimetre vertical resolution by incorporating sedimentological, ichnological and palaeontological observations. Samples have been collected when appropriate in order to enable thin-section analysis of key carbonate lithofacies. Although palaeocurrent azimuth directions were measured on aeolian and tidal dune foresets, their comprehensive analysis is outwith the scope of this study. Correlations between these logs have been made based upon the assumption that the sequence-stratigraphic framework discussed in this work, and its associated system tracts bounding surfaces, are ubiquitously expressed throughout the exposure of the Carmel Formation within the studied area. Vertical facies dislocations have been used to define maximum flooding surfaces (MF) and maximum regressive surfaces (MR). Furthermore, this stratigraphic framework is built upon the hypothesis that sediment distribution on a regional scale was disconnected from Middle Jurassic thrusting activities of the Cordilleran orogen to the west of the Utah-Idaho Trough. Indeed, regional accommodation creation during the studied interval was generated through constant subsidence during a period of tectonic quiescence in between thrusting events (Bjerrum & Dorsey, 1995). Effects of localised bulging events of the Monument Upwarp (Havholm *et al.*, 1993) onto the accommodation of the documented parts of the basin aren't considered in this study.

Markov chain analyses depicting the stratal disorder of the tidal sediments of the Carmel Formation have been conducted on three neighbouring sections in the San Rafael Swell area where successions are dominantly composed of sub- to supratidal sediments (Sections 1 to 3, Fig. 2). Observed stratal signals of these analysed sections are considered representative of a region where facies distributions were not impacted by aeolian processes of the Page Sandstone erg. Statistical evaluation of stratal transitions based on the method introduced by Burgess (2016) enabled the generation of transverse probability matrices for both facies and facies associations. A total of six Markov metric values were calculated through diagonal summations of transition probability matrices for both facies and associations for each of the three selected logs. These Markov metric values were compared on kernel density plots of the density distributions of stochastically shuffled successions based on each section's sedimentological diversity. Order or disorder of a given succession is statistically evaluated by comparing its unique Markov metric value to the distribution of values from disordered successions.

The facies scheme discussed in this study is applied to satellite images (ESRI World Imagery) of the Adair Bay, Mexico, in order to provide high-resolution plan view facies distribution interpretations compatible with the results of this analysis. The Adair Bay is described as an arid fluvially starved tidal embayment bordered by the Gran Desierto dune field (Beveridge *et al.*, 2006; Scheidt *et al.*, 2011). Because of its nature and its significant scale (~500 km^2), the Adair Bay is considered as a good modern analogue for the Carmel Formation. In addition to a complete map of the embayment, three localised maps have been produced to highlight key plan view facies interactions ultimately leading to architectural complexities within the depositional elements discussed in the proposed model.

FACIES ANALYSIS OF THE CARMEL FORMATION

Twenty-five lithofacies are recognised in the Carmel Formation and are related to a wide range of aeolian processes, tidal dynamics and open-marine processes (Table 1). Sedimentary facies have been grouped into 11 associations representing the products of co-occurring processes (Table 2; Figs 3 to 13).

Aeolian facies associations

Dry aeolian dune association (FA1)

Description. The dry aeolian dune association (Fig. 3) is the most continental deposit identified in this work and is composed of lithofacies Axs, Atxs, Ahl, Air and Acl (Table 2). It is typically characterised by metre-scale cross-stratified sets of reverse-graded dune foreset avalanching deposits (grainflow), coupled with drapes of settled suspended load (grainfall) (Fig. 3A). These units can either depict tabular and laterally extensive decametre-scale cross-stratification

Table 1. Summary of lithofacies observed in the aeolian to marine-dominated transition of the Carmel Formation.

Code	Facies	Texture	Structures	Processes
Axs	Straight cross-stratified aeolian sandstone	Grey to yellow fine to coarse-grained, well-sorted, well-rounded, clast-supported quartz grains	Laterally continuous cross-stratification sets (1–30 m thick) with bimodal grain-size foreset couplets, truncated by reactivation and superimposition surfaces	Episodic gravity-driven avalanching events on the lee-slope of straight-crested migrating aeolian dune-forms (i.e. grain flow) during continuous settlement of suspended load (i.e. grain fall)
Atxs	Trough cross-stratified aeolian sandstone	Grey to yellow fine to coarse-grained, well-sorted, well-rounded, clast-supported quartz grains	Trough cross-stratification sets (1 to 30 m thick) with bimodal grain-size foreset couplets. 'Scour and fill' geometries and occasional preservation of small bedform top sets	Episodic gravity-driven avalanching events on sinuous crested migration aeolian dune-form lee slope (i.e. grain flow) during continuous settlement of suspended load (i.e. grain fall)
Arxs	Reworked cross-stratified aeolian sandstone	Grey to yellow very fine to medium-grained poorly to well-sorted, sub- to well-rounded, clast-supported quartz grains	Laterally continuous to trough cross-stratification sets (1 to 5 m thick) with contorted bimodal grain-size foreset couplets. Soft sediment deformation, truncated topsets with decimetre-scale dune-form cross-stratifications sets and occasional oscillation ripple cross-lamination and desiccation cracks	Aeolian dune-forms migrating under high watertable conditions and subject to subaqueous reworking
Aha	Haloturbated aeolian sandstone	Grey to yellow medium to coarse-grained, well to moderately sorted, well-rounded, clasts supported quartz grains	Laterally continuous to trough cross-stratification sets (1 to 5 m thick) with contorted bimodal grain-size foreset couplets. Truncated topsets with irregular highly cemented and laterally extensive top bounding surface. Metre-scale polygonal fractures with intense soft sediment deformation, occasional rhizoliths, burrows and chert concretion	Dampened and fractured aeolian deposits by secondary evaporitic crust surface generation related to watertable salt precipitation
Ast	Structureless and deformed aeolian sandstone	Yellow to pale red fine to medium-grained, moderately sorted, well-rounded, clast-supported quartz grains	Structureless sandstone (1 to 5 m thick) with bleached and contorted strata. Occasional water escape structures, microfaulting and oxidised indurated top surfaces	Contorted water-saturated aeolian sediment with intense burial-induced deformation

Table 1. (continued)

Code	Facies	Texture	Structures	Processes
Ahl	Horizontally laminated aeolian sandstone	Grey to yellow medium to coarse-grained, moderately to well-sorted, sub-rounded, clast-supported quartz grains	Pinstripe lamination sets (<2 m thick) with occasional impact ripple lamination	Vertically aggrading windblown sediment on a flat dry surface
Air	Impact ripple cross-laminated aeolian sandstone	Grey to yellow very fine- to fine-grained, well-sorted, well-rounded, clast-supported quartz grains	Impact ripple-laminated sandstone (<2 m thick) interfingering with facies Axs and Atxs	Suspended load settlement and migrating impact ripples on aeolian dune plinth
Acl	Crinkly laminated aeolian sandstone	Yellow to rusty orange, very fine to medium-grained, well-sorted, well-rounded, clasts supported quartz grains	Isolated crinkly to undulating planar laminated sandstone (<2 m thick) with adhesion structures and vertically aggrading wavy cryptalgal mat	Suspended load trapping on a dampened or wet surface
Smo	Mottled silicoclastic sabkha	Rusty orange to reddish, very fine to medium-grained, poorly to well-sorted, well-rounded, clasts supported quartz grains	Extensive crinkly to undulating planar laminated sandstone (1 to 5 m thick) with heterolithic grain-size distribution. Intense mottling and soft sediment deformation	Vertically aggrading windblown sediment on a dampened surface subject to strong burial deformation
Sev	Crystalline evaporites	Isolated white to pale green crystalline gypsum and anhydrite beds with enterothic folds	Highly contorted layered units (1 to 10 m thick)	Salt precipitation on evaporitic sabkha playa
Fcl	Desiccated clay	Dark red to pinkish clay	Infilled desiccation cracks (1 to 10 cm wide)	Clay deposition in null bed shear-stress conditions
Mdo	Microbial dolomicrite	Light-yellow to reddish interbedded silts to very fine quartz grains and dolomicrite	Columnar stromatoliths to stratiform cryptalgal dolomicrite lamination sets (0.5 to 5 m thick) with smooth crested oscillation ripple cross-lamination	Microbially induced carbonate precipitation coupled with the trapping of terrigenous material in very shallow water depths
Mosc	Oscillatory ripple cross-laminated sandstone	Light-yellow very fine to fine-grained, well to moderately sorted, well to sub-rounded, clasts supported quartz grains. Rare bioclasts (echinoids and bivalves)	Sand-dominated heterolithic stratification sets (0.5 to 5 m thick) with bifurcating to ladderback oscillation ripple forms exposed in plan view. Occasional very high ichnological index (*Cruziana* ichnofacies) and nodular gypsum. Interbedded with Fcl	Subaqueous grains entrainment by oscillating current direction

Table 1. (continued)

Code	Facies	Texture	Structures	Processes
Mmic	Oncoidal packstone	Light-yellow oncoidal and pelloidal packstone with quartz grains nuclei	Thinly laminated and oscillation ripple cross-laminated packstone (1 to 10 cm thick). Interbedded with Mosc and Mmud	Rolling and reworking of soft microbial mat and faecal clasts
Mmud	Carbonate mudstone	Light grey mudstone	Structureless carbonate mudstone (0.1 to 1 m thick) with rare *Cruziana* ichnofacies	Clay-size carbonate clasts settlement in null bed shear-stress conditions
Mmar	Plane bedded marls	Pale blue grey mudstone (50%) and light green clay (50%)	Thick and extensive plane-bedded units (1 to 10 m thick)	Mixed terrigenous clay and carbonate mud particles settlement in null bed shear-stress conditions
Mfen	Fenestral fabric	Light grey pelloidal wackestone to packstone	Extensive wackestone to packstone unit (0.5 to 2 m thick) with quartz-recrystallised fenestral fabric	Reworked faecal clasts and remnant porosity inherited by microbially induced gas trapping
Mxs	Cross-stratified to structureless oolitic grainstone	Light grey oolitic and bioclastic wackestone to grainstone	Extensive cross-stratified wackestone to grainstone sets (0.5 to 2 m thick) with occasional reactivation surfaces, bidirectional foresets azimuths and lenses of accumulated bioclastic debris. Presence of mud drapes at cross bedding toesets. Occasionally observed as thin structureless beds (10 to 50 cm thick)	Subaqueous dune migration under bidirectional Newtonian flow with highly variable bed shear-stress
Mbw	Laminated bioclastic wackestone	Light grey bioclastic wackestone	Thick plane bedded and laminated wackestone (1 to 10 m thick) with occasional vertical burrows and trace fossils	Subaqueous fine carbonate particles settling in calm conditions disrupted by bioclastic deposition during rare higher energy events
Mhb	Herringbone ripple cross-laminated sandstone	Light-yellow very fine-grained, well-sorted, clasts supported, quartz grains	Isolated herringbone cross-stratified sandstone (0.2 to 1 m thick) with *Skolithos* ichnofacies	Subaqueous ripple migration under bidirectional turbulent Newtonian flow
Mlxs	Low-angle cross-stratified sandstone	Light-yellow very fine-grained, well-sorted, clast-supported quartz grains	Extensive low-angle cross-stratified sandstone (0.5 to 2 m thick) with occasional upper flow regime parallel lamination and rare oscillatory ripple cross-lamination. Often associated with Mhcs	High-energy and multi-directional subaqueous sediment remobilisation

Table 1. (continued)

Code	Facies	Texture	Structures	Processes
Mhcs	Hummocky cross-stratified sandstone	Light-yellow very fine to fine-grained, moderately to well-sorted, sub-rounded, clast-supported quartz grains	Hummocky and swaley cross-stratified sandstone (10 to 30 cm thick)	Subaqueous grains entrainment by the superimposition of mutlidirectional currents
Mhg	Encrusted hardground	Rusty brown medium to coarse-grained, sub-angular, poorly sorted, clast-supported, quartz grains and bioclastic debris	Structureless concentration layers (<50 cm thick) of oriented and disarticulated shells with highly oxidised top surfaces	Rapidly decreasing high bed shear stress events depositing large amount of bioclasts followed by long periods of non-deposition
Mstl	Structureless marine sandstone	Beige very to fine-grained, sub-rounded to sub-angular, moderately sorted, clast-supported quartz grains with rare bioclastic content	Structureless to crude cross-stratified sandstone (0.5 to 2 m thick) with erosive base, irregular bedding surfaces and strongly cemented. Occasional burrows	Diagenetically altered subaqueous bedform migration under turbulent Newtonian flow with occasional bioturbation
Msto	Heterogeneous bioclastic strata	Grey fine to medium-grained, sub-rounded to angular, poorly sorted, matrix-supported quartz grains and bioclasts	Heterogenous structureless sandstone (0.5 to 2 m thick) with bioclastic-rich alignment layers. Numerous rounded mud balls	Subaqueous high sediment load deposition with sudden drop in shear stress

Table 2. Summary of facies associations with their contained lithofacies, brief descriptions and supporting references.

Code	Facies association	Facies included	Description	References
FA1	Dry aeolian dune	Axs, Atxs, Ahl, Air, Acl	Aeolian dune field composed of straight-to-sinuous crested transverse dunes and compound superimposed draa separated by watertable-controlled dry to wet interdune corridors	Hunter (1977), Kocurek & Dott (1981), Mountney & Thompson (2002)
FA2	Wet aeolian dune	Arxs, Aha, Ast, Acl	Coastal barchanoid dune field encroaching over a tidally influenced sabkha surface (FA3). Subject to wave breaching and tidal reworking	Kocurek (1981b), Blakey & Middleton (1983), Fryberger *et al.* (1983), Chan (1989), Fryberger *et al.* (1990), Rodríguez-López *et al.* (2012); Lokier (2012)
FA3	Evaporitic sabkha	Acl, Smo, Sev	Evaporitic coastal sabkha characterised by large disconnected hypersaline ponds occasionally flooded by high tides	Kinsman (1969), Kendall (1978), Andreason (1992), Alsharhan & Kendall (2003)
FA4	Upper intertidal microbialite	Mdo, Mxs	Extensive microbial mats represent the maximum mean high-tide elevation zone of the tidal flat. Occasionally observed as columnar stromatoliths buried under oolitic sand carried inland during storm events	Eriksson & Truswell (1974), Quijada *et al.* (2020), Ferronatto *et al.* (2024)
FA5	Lower intertidal siliciclastic heterolithic flat	Fcl, Mosc	Fining-landward sand- to mud-dominated lower intertidal heterolithic flat controlled by tidal cyclicity and subject to aerial exposure. Externally sourced from the flanking marginal dune fields (FA1 and FA2) and potentially ephemeral fluvial pulses	Reineck & Wunderlich (1968), Chakrabarti (2005), Zuchuat *et al.* (2018), Wroblewski & Schueth (2023)
FA6	Subtidal mixed carbonate –siliciclastic flat	Mosc, Mmic, Mmud	Fining-landward grainstone- to mudstone-dominated mixed subtidal flat influenced by tidal cyclicity. Locally sourced from microbially and chemically induced carbonate productions coupled with the input of oncoidal and pelloidal material during higher energy events	Demicco (1983), Védrine *et al.* (2007), Hashmie *et al.* (2016)
FA7	Restricted lagoon	Mmar, Mfen, Msto, Mstl	Calm and restricted lagoonal bay protected from the waves, prone to preserving fine marly material. Surrounds tidal channel fills (FA12). Occasionally, it records the deposition of bioclastic storm deposits	Shinn (1983), Einsele & Ricken (1991), Steel *et al.* (2012)

Table 2. (continued)

Code	Facies association	Facies included	Description	References
FA8	Sandy tidal channel-fill	Mhb, Mstl	Tidal channel-fill comprising sandy deposits of sudden high sediment loads and bidirectional bedform cosets deposited under alternating confined channelised tidal current. Interbedded with FA6 and FA7	Visser (1980), Allen & Homewood (1984), Lanier & Tessier (1998)
FA9	Oolitic tidal dune	Mxs, Mbw, Mhb	Compound tidal dune composed of oolitic sand and bioclastic material. Part of a shoal complex prone to strong tidal currents	Gonzalez & Eberli (1997), Olariu *et al.* (2012), Rankey & Reeder (2012)
FA10	Wave-dominated shoreface to foreshore	Mlxs, Mhcs, Mstl	Laterally extensive wave-dominated foreshore and beach swash-zone deposits associated with barrier islands and sand spits	McCubbin (1982), Duke (1985), Cheel & Leckie (1993), Dalrymple & Rivers (2023)
FA11	Offshore transition	Mmud, Mmar, Mbw, Mhg	Bioclastic tempestite layers deposited below the fair-weather base and are interbedded with marls in the offshore transition zone. Bioclastic material is derived from FA9	Wilson & Palmer (1994), Myrow & Southard (1996), Rodrigues *et al.* (2024)

sets (Axs) or more three-dimensional trough and amalgamated cross-stratification sets (Atxs; Fig. 3E). Grainflow strata interfinger at the tosets of dune lee slopes with impact ripple cross-lamination sets (Air; Fig. 3D) or crinkly laminated very fine to silty deposits (Acl; Fig. 3C). Vertical stacking of horizontal laminations (Ahl), characterised by strong bimodal grain-size distributions, are sporadically present along with impact ripple cross-laminations (Air).

Interpretation. These lithofacies together record the migration of aeolian bedforms (Hunter, 1977; Kocurek & Dott, 1981). Preserved architectural differences in cross-strata (Axs & Atxs) reflect variations in aeolian dune morphology. While straight-crested transverse dunes tended to be recorded as tabular cosets of laterally continuous cross-bedded sets, sinuous dunes represent cosets of complex internal geometric relationships (Rubin & Hunter, 1982). Highly amalgamated aeolian dune sets (i.e. scour-and-fill; *sensu* Cardenas *et al.*, 2019) are associated with localised wind turbulence caused by the increasing complexity of dune morphologies toward the erg centre. Impact ripple cross-laminated and crinkly laminated sets (Air and Acl) are associated with interdune corridors characterised by variable dampness conditions on the sediment surface (Mountney, 2006). The migration of impact ripples (Air & Acl) alongside aeolian dunes generated interdune migration surfaces that bounded aeolian dune cross-stratification sets (Fig. 3E; Kocurek, 1981b; Mountney & Thompson, 2002). Vertically stacked bimodal lamination deposits (Ahl) are interpreted as aggrading bedform-free dry aeolian sandsheet surfaces covered with impact ripples (Kocurek & Nielson, 1986).

Tidally reworked wet aeolian dune association (FA2)

Description. The tidally reworked wet aeolian dune association (Fig. 4) is composed of diverse lithofacies linked to depositional processes of differing nature (Arxs, Aha, Ast and Acl; Table 2). The association is primarily characterised by the co-occurrence of metre-thick convoluted aeolian cross-stratification sets sporadically displaying subaqueous reworking features such as oscillatory ripple cross-lamination and structureless to cross-stratified decimetre-thick subaqueous strata with sharp erosive bases (Arxs; Fig. 4A, E and F). Both subaerial and subaqueous cross-stratification sets occur within the overall same lithology (cf. facies Axs/Atxs in FA1). Heavily contorted and deformed aeolian sandstone units (Ast) reveal water-saturated conditions in these sediments by the time of deposition (Fig. 4D). Tidally reworked wet aeolian dune associations are typically capped by contorted aeolian cross-stratification sets penetrated and brecciated by metre-scale sandy polygonal fracture-fills (Aha; Fig. 4B and C).

Interpretation. The characteristic coexistence of sedimentary structures linked to contrasting aeolian and subaqueous processes records the preservation of coastal dunes subject to reworking and breaching by tidal currents. Similar facies have been reported in both ancient marginal aeolian deposits (Blakey & Middleton, 1983; Chan, 1989) and modern coastal dune fields (Fryberger *et al.*, 1983, 1990). The absence of grainflow-grainfall couplets and the occurrence of oscillatory sedimentary structures in subaqueous strata (Arsx) betray the presence of standing shallow-water bodies that partly reworked isolated aeolian bedforms migrating across the supratidal flat (Axs & Atxs). Crinkly laminated sandstones (Acl) are attributed to the trapping of windblown sediment onto dampened surfaces during ebb tide. Heavily contorted sandstone units (Ast) are interpreted as water-saturated aeolian dunes subject to intense deformation caused by water escape processes on burial, rather than the result of syn-depositional folding by simple slumping of dune toe sets. Finally, fractured aeolian units (Aha) are interpreted to reflect the development of evaporitic crusts through salt precipitation during erg deflation events coupled with a high water table (Kocurek & Hunter, 1986; Lokier, 2012). This association marks the transition from erg-centre successions dominated by dunes (FA1) to tidal flat environments.

Tidal facies associations

Supratidal evaporitic sabkha association (FA3)

Description. The evaporitic sabkha facies association (Fig. 5) is the only representative of the supratidal facies belt of the Carmel Formation, and it is ubiquitously present along its exposure across the Colorado Plateau. It is composed of lithofacies Acl, Smo, Fcl and Sev (Table 2). The association is dominated by crystalline gypsum deposits (Sev) varying in extent from localised

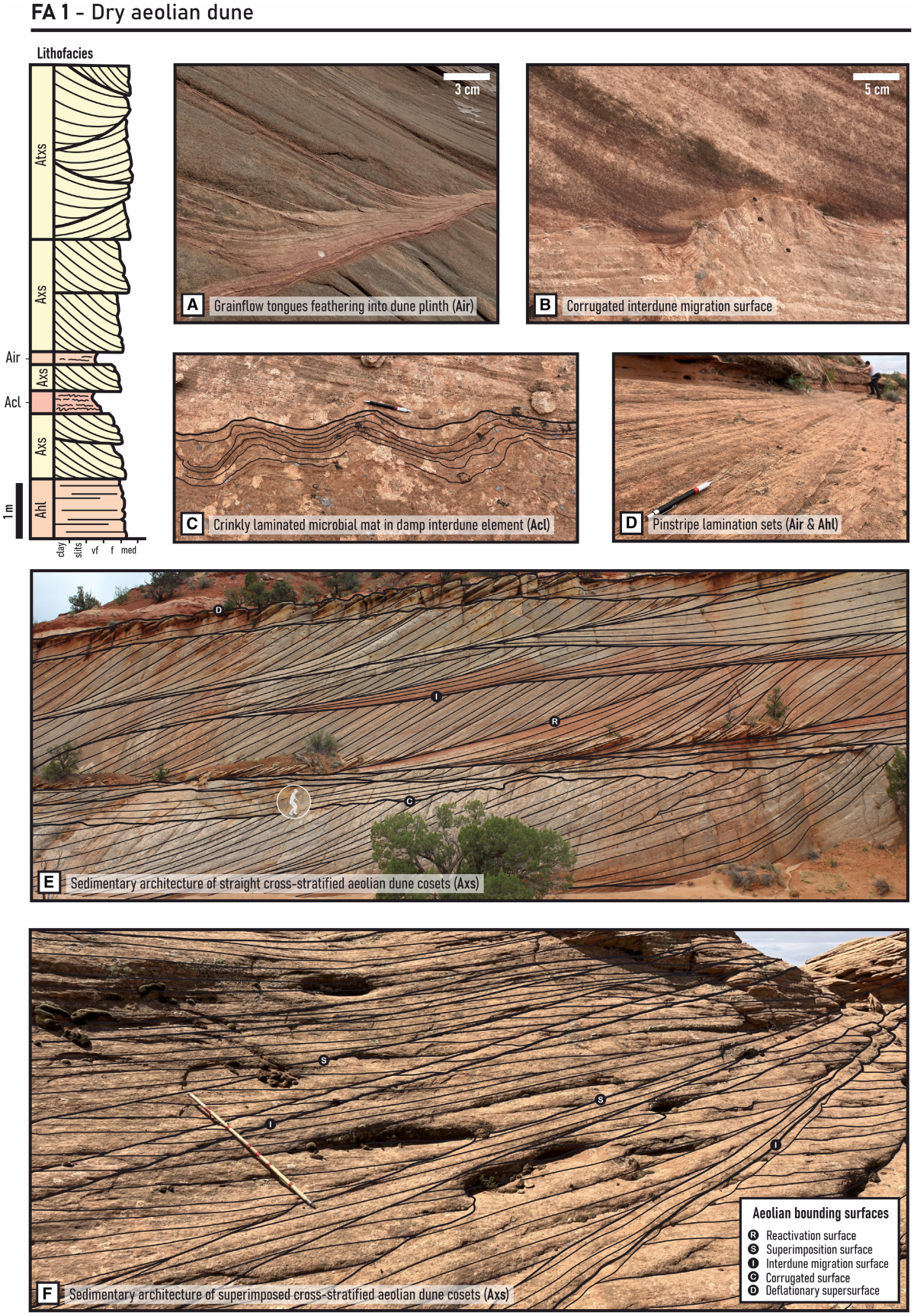

Fig. 3. Lithofacies diversity of dry aeolian dune association (FA1). (A) Feathering pattern between grainflow deposits and impact ripple laminations (Air). (B) Corrugated interdune migration surface linked to water table fluctuations at the time of deposition. (C) Crinkly laminated damp interdune deposits (Acl) with undulating microbial mat structures. (D) Impact ripple cross-laminations (Air). (E) Tabular cross-stratified aeolian dune coset (Axs) displaying various bounding surfaces of different orders. (F) Superimposition surfaces with a cross-stratified aeolian dune coset (Axs). The suggested vertical facies distribution represents the idealised sequence of a maturing and drying-upward dune field.

decametre-scale lenses to extensive kilometre-scale layers interbedded within reddish mudstone units (Fcl; Fig. 5A). Evaporite beds often record internal centimetre-scale precipitation as microfolded crystalline laminations (i.e., enterolithic folds) (Fig. 5A and B). Mottled siliciclastic sabkha facies (Smo) are sporadically present and differ from Ast facies by the absence of aeolian structures and the presence of convoluted laminations and plume features.

Interpretation. The facies of this association are interpreted together as the product of water table-controlled salt precipitation in the supratidal facies belt. Precipitation of crystalline gypsum occurred interstitially within the pore spaces between siliciclastic material and generally translated landward into nodular anhydrite belts (Sev) in the groundwater capillary fringe (Kinsman, 1969; Wood & Wolfe, 1969; Kendall, 1978; Pettigrew *et al.*, 2021). The inconsistent lateral extent of evaporite beds, as well as their spatial distribution, suggests that their deposition was substantially controlled by autocyclic factors (Clement & Holland, 2016). In the case of siliciclastic-rich coastal sabkha environments, soft sediment deformation structures in sandy units (Smo) derived from high-tide beach material are associated with dewatering and haloturbation processes (Andreason, 1992). Crinkly laminated sandstones (Acl) are interpreted as windblown sediment trapped upon dampened supratidal surfaces, while reddish mudstones (Fcl) are associated with the settlement of clay particles within standing water ponds.

Upper intertidal microbialite association (FA4)

Description. The microbialite association (Fig. 6) is dominated by intertidal deposits composed of lithofacies Mdo and Mxs (Table 2). It is mainly characterised by millimetre-scale laminated couplets of micritic mudstone and very fine sand affected by secondary dolomitisation (Mdo; Fig. 6C). Couplets are typically observed as extensive kilometre-scale units of wavy to crinkly laminated sets which may sporadically display ripple-form shapes (Fig. 6D). Sporadically, microbialites are found interbedded with structureless oolitic sand (Mxs) and they may develop as decimetre-high columnar stromatolites (Fig. 6A). In this latter case, microbialite clasts can be reworked and deposited as floating clasts in oolitic sand (Fig. 6B).

Interpretation. Microbialite facies observed in the Carmel Formation are the result of biologically induced carbonate precipitation associated with the trapping and binding of siliciclastic grains in low-energy settings (e.g. Suarez-Gonzalez *et al.*, 2019; Harris *et al.*, 2024). Laminated couplets of micritic mudstone and very fine sand (Mdo) were deposited by extensive algal mats restricted to the upper intertidal zones (Evans, 1966; Kendall & Skipwith, 1969; Court *et al.*, 2017). This facies is similar to modern microbial mats observed in coastal deposits of the southern Arabian Gulf (Kenig *et al.*, 1990; Alsharhan & Kendall, 2003). Wavy to crinkly morphologies are interpreted as tufted microbial mats overlying ripple-forms commonly known as palimpsest ripples (Eriksson & Truswell, 1974; Sarkar *et al.*, 2016). Despite these sediments being dominantly associated with very calm energy settings, occasional storm events may have disrupted microbial mat areas by dismantling parts of them and generating thrombolites (Paul *et al.*, 2021). In a similar fashion, oolitic material (Mxs) derived from open-marine oolitic factories (FA9) was sporadically brought landward to the intertidal facies belt during high-energy events and interbedded as structureless beds within microbialite strata.

Lower intertidal heterolithic siliciclastic flat association (FA5)

Description. The heterolithic siliciclastic flat association (Fig. 7) represents a depositional area where evidence of both subaerial exposure and subaqueous transport is equally preserved, but with carbonate precipitation absent. It is composed of lithofacies Fcl and Mosc (Table 2).

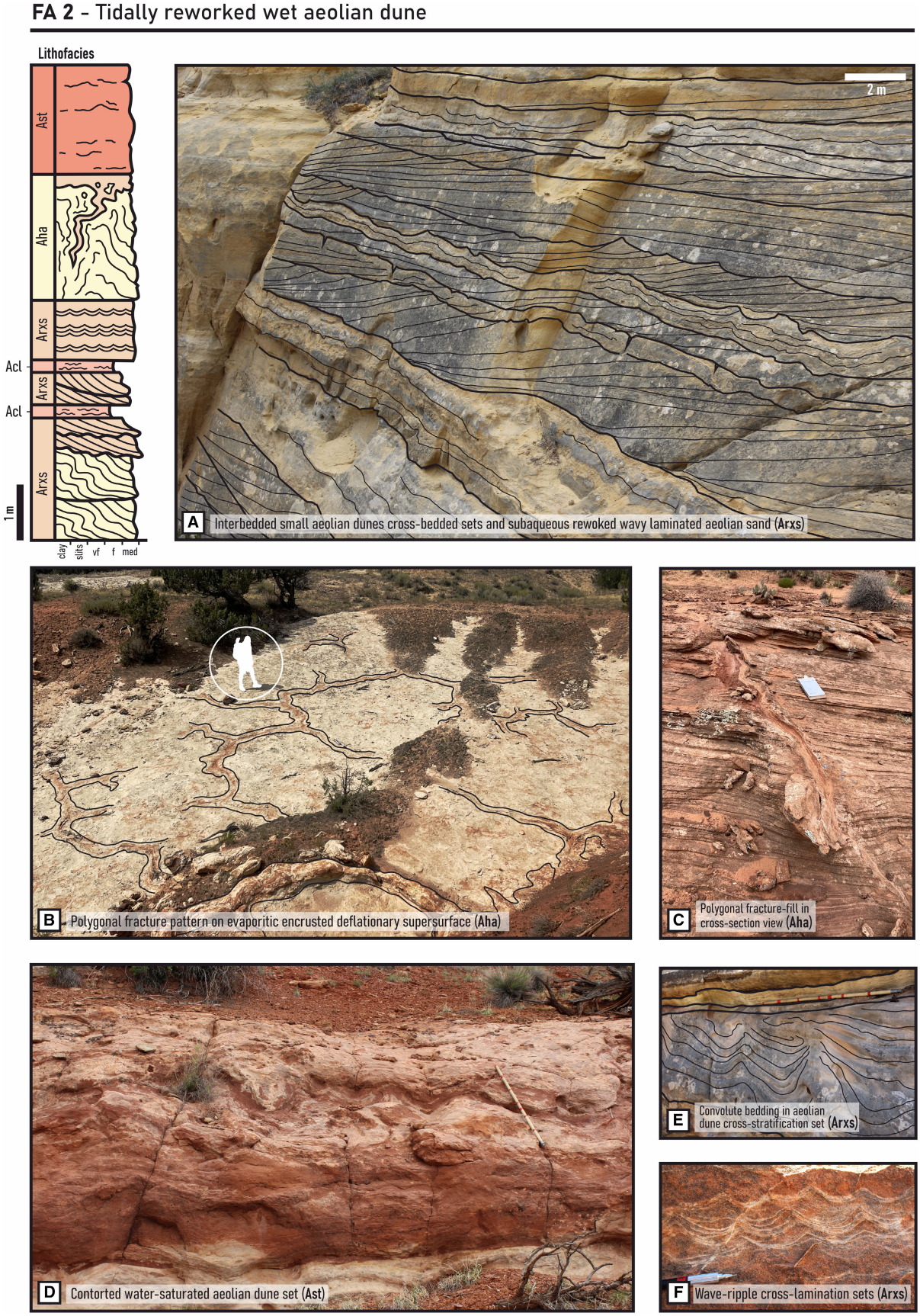

Fig. 4. Lithofacies diversity of tidally reworked wet aeolian dune association (FA2). (A) Interbedded small aeolian cross-stratification sets and subaqueous strata (Arsx). (B) Polygonal fracture plan view pattern on an aeolian deflationary surface (Aha). (C) Focus on a polygonal fracture fill cross-section penetrating underlying aeolian set (Aha). (D) Water-saturated aeolian dune displaying heavily contorted strata. (E) Soft sediment deformation in aeolian dune set. (F) Oscillation ripple cross-laminations in tidally reworked aeolian material. The suggested vertical facies distribution represents the idealised sequence of a coastal aeolian dune field undergoing a deflationary stage.

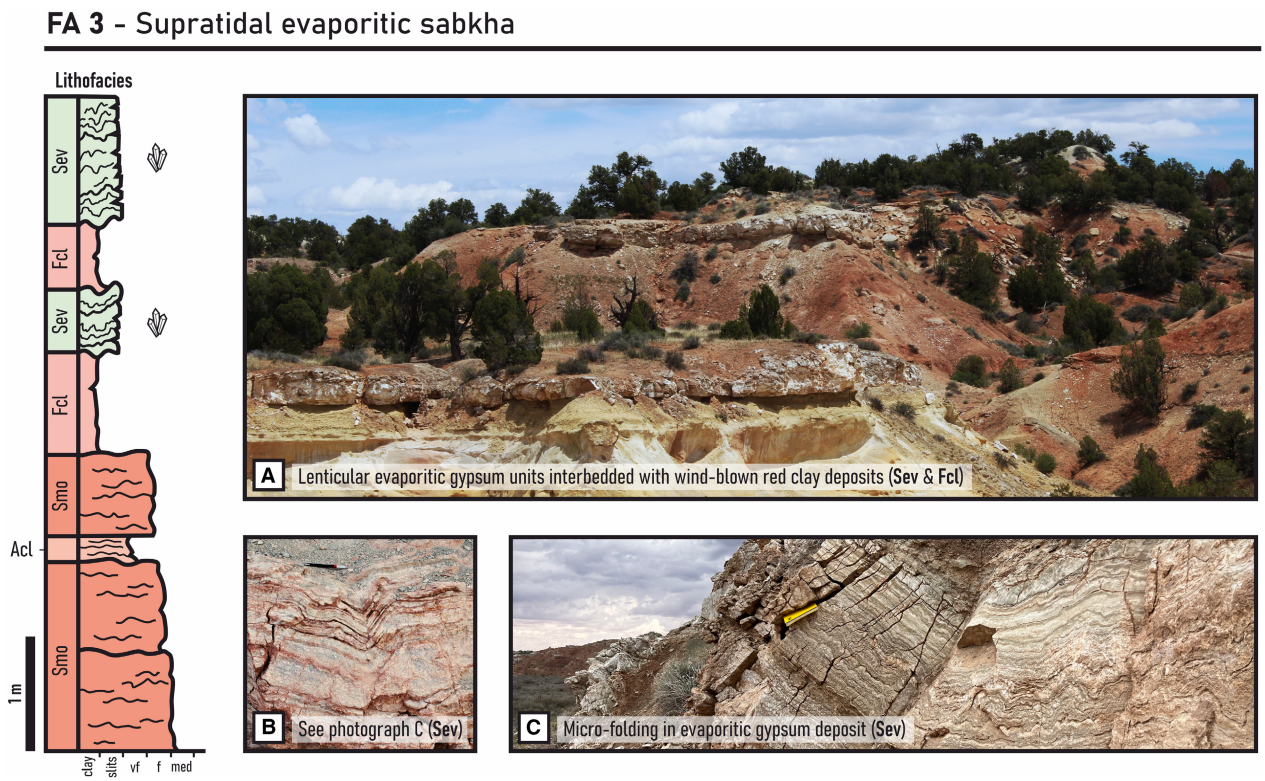

Fig. 5. Lithofacies diversity of supratidal evaporitic sabkha association (FA3). (A) Sedimentary architecture of lenticular evaporite beds (Sev) interbedded in red mudstone units (Fcl). (B) Detailed photograph of a folded anhydrite bed (Sev). (C) Haloturbation and enterolithic folds in evaporite unit (Sev). The suggested vertical facies distribution represents the idealised drying-upward sequence of a coastal sabkha.

Desiccated red clay (Fcl) and oscillatory ripple-laminated fine sand (Mosc) in various ratios describe a continuous range of heterolithic stratification from flaser, to wavy and to lenticular bedding (Fig. 7A to D). Oscillatory ripple-laminated fine sand is sporadically characterised by a high bioturbation index with abundant *Gyrochorte* (Fig. 7F) and *Skolithos* trace fossils (Fig. 7G). *Thalassinoides* and *Asterosoma* (Fig. 7E and H) traces are sporadically observed. Oscillatory ripple-form crest-lines are generally straight and rounded (Fig. 7A) and sporadically display interference patterns.

Interpretation. Facies of the association are interpreted together as the lower intertidal record of siliciclastic sediment transport and deposition under fluctuating tidal flow, coupled with the settling of clay particles and subaerial exposure during high and low tides, respectively. Heterolithic stratification sets are generally associated with fining-landward successions (Reineck & Wunderlich, 1968), but various localised mechanisms may influence the preservation of such sedimentary successions (e.g. Longhitano *et al.*, 2014; Zuchuat *et al.*, 2019). Ripple-forms in plan view (Mosc) can vary in

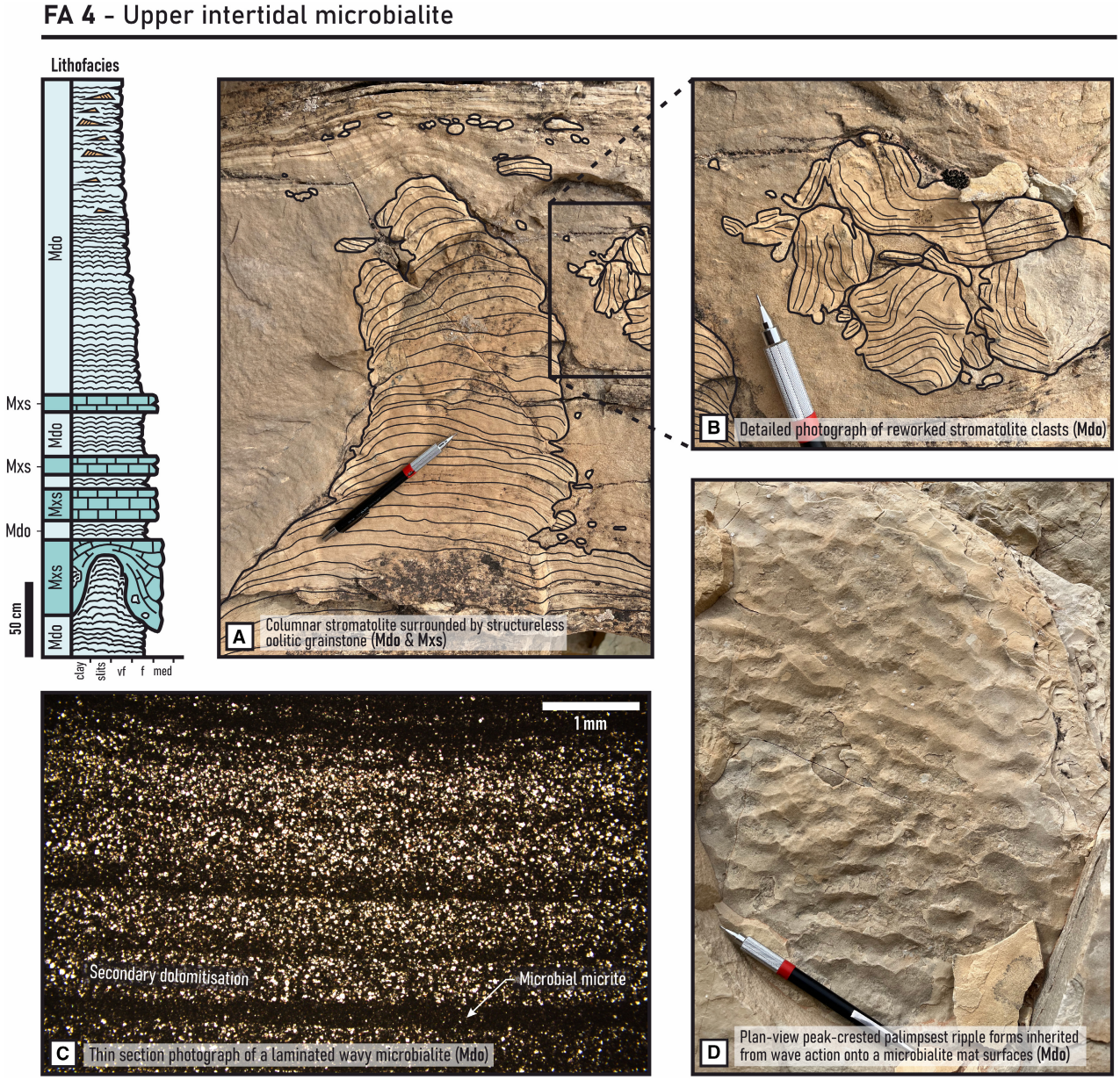

Fig. 6. Lithofacies diversity of microbialite facies association (FA4). (A) Columnar stromatolite (Mdo) embedded in structureless oolitic grainstone (Mxs). (B) Details of a reworked microbialite clasts. (C) Thin section photograph illustrating microbial dolomicrite. (D) Plan view microbial mat view displaying peak-crested oscillation ripple form morphologies associated with wind action on the shore of restricted ponds. The suggested vertical facies distribution represents the idealised shallowing-upward sequence of a coastal microbialite.

Fig. 7. Lithofacies diversity of heterolithic siliciclastic flat facies association (FA5). (A) Centimetre-scale desiccation cracks of clay drapes facies (Fcl) in oscillatory ripple troughs (Mosc). (B) Sand-dominated flaser bedding (Mosc). (C) Desiccated clay (Fcl). (D) Mud-dominated lenticular bedding (Mosc and Fcl). (E) Thalassinoides bottom plan view (Mosc). (F) Gyrochorte top plan view (Mosc). (G) Skolithos bottom plan view (Mosc). (H) Asterosoma bottom plan view (Mosc). The suggested vertical facies distribution represents the idealised shallowing upward sequence of a siliciclastic heterolithic flat.

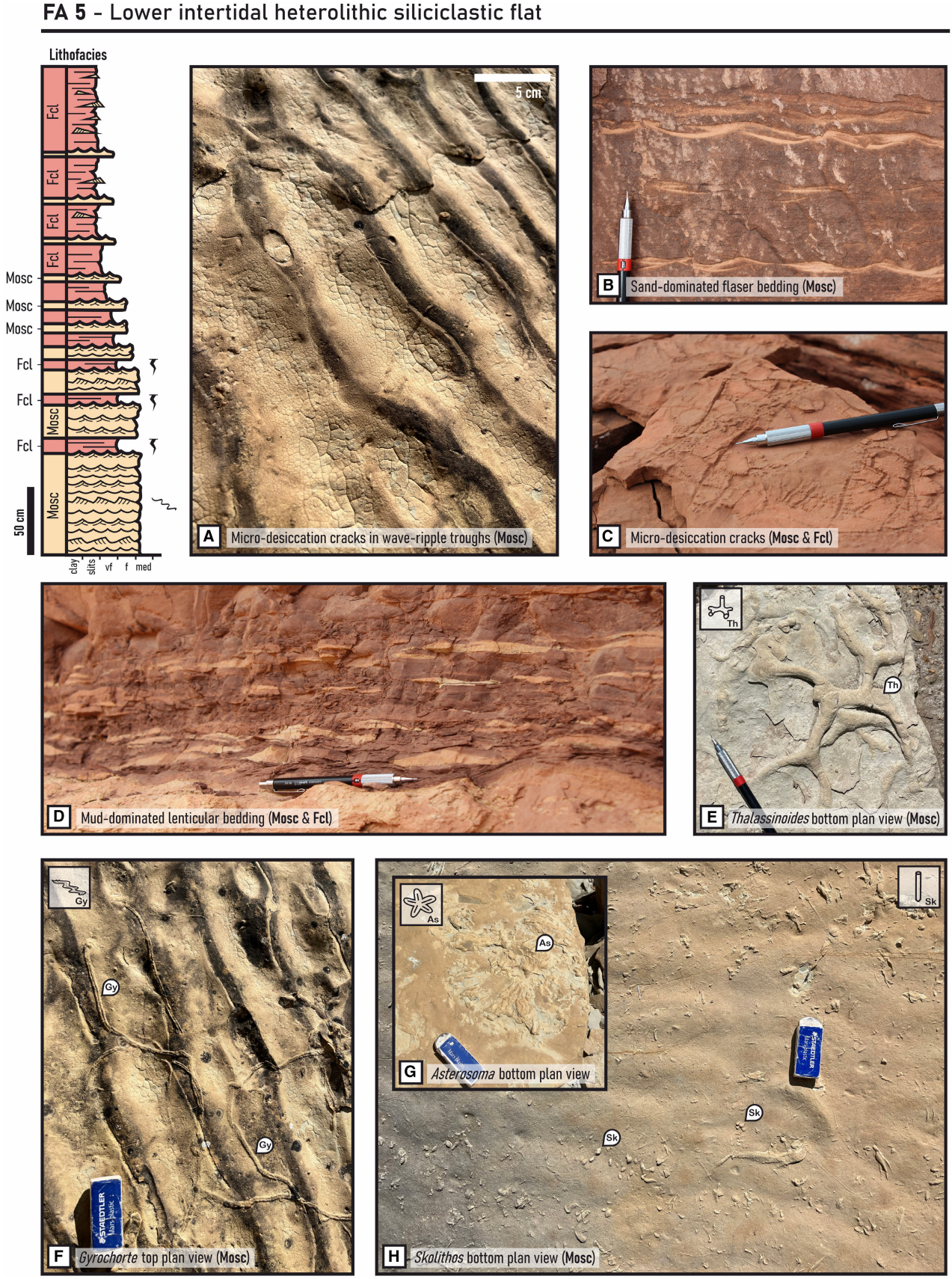

morphology, symmetry and migration direction due to the strong autogenic aspect of heterolithic flats (Chakrabarti, 2005). The purely siliciclastic nature of FA5 is interpreted as the localised expression of aeolian sand flux into the tidal flat, coupled with occasional ephemeral-fluvial pulses that reached the coastal plains. The sporadically high ichnological abundance in oscillatory ripple-laminated fine sand (Mosc) shows similarities with siliciclastic tidal successions stratigraphically related to the Carmel Formation (e.g. De Gibert & Ekdale, 2002; Wroblewski & Schueth, 2023) and may reflect localised lower rates of sedimentation in more protected areas of the intertidal facies belt.

Subtidal mixed carbonate–siliciclastic flat association (FA6)

Description. The subtidal mixed carbonate–siliciclastic flat association is composed of lithofacies Mosc, Mmic and Mmud (Table 2). In a similar fashion to the lower intertidal siliciclastic heterolithic flat association (FA5) (Fig. 8), it is characterised by heterogeneous grain-size deposits forming a wide range of flaser to lenticular bedding. Distinction between the two associations lies in their lithological differences and in the absence of facies from FA6 that provide evidence for subaerial exposure. The association comprises three different lithofacies linked to variable sediment sources and depositional processes. Micritic lime mudstones (Mmud) are deposited in very low hydrodynamic conditions favourable to the development of trace fossils (Fig. 8A, F and G) and are typically interbedded with sandy ripple-laminated strata (Mosc), which suggests regular siliciclastic sediment flux into the subtidal carbonate factory (Fig. 8A to D). In addition, sporadic micritised oolitic grainstone beds (Mmic) can be observed draping preserved bedforms (Fig. 8E). Micritised ooids are developed from quartz grain nuclei and can be observed with occasional well-rounded millimetre-scale intraclasts (Fig. 8H and I).

Interpretation. The association is interpreted as the sedimentary expression of a shallow carbonate subtidal flat affected by siliciclastic pulses and wave action. Micritic mud (Mmud) is associated with periods of low bed shear stress during slack tides, while ribbons of lenticular to wavy siliciclastic bedding (Mosc) were deposited during periods of tidal current (e.g. Demicco, 1983; Lasemi *et al.*, 2012; Hashmie *et al.*, 2016). The development of micritised ooids (Mmic) is associated with the coating of lithoclast nuclei by microbial laminae growth. Their well-rounded morphologies and the presence of intraclasts suggest occasional transport and deposition through wave action during storm events. FA6 is generally considered as part of the subtidal facies belt as carbonate production cannot be sustained under episodic aerial exposure of the intertidal facies belt.

Restricted lagoon association (FA7)

Description. The lagoon facies association (Fig. 9) is linked to sedimentation under very low-energy levels in the subtidal system and comprises the lithofacies Mmar, Mfen, Msto and Mstl (Table 2). It is mainly composed of decametre-thick but kilometre-scale units of tabular blue marls (Mmar; Fig. 9A and C). Sporadic occurrences of peloidal grainstone units with fenestral fabric (Mfen; Fig. 9B) betray exceptional subaerial exposure (Shinn, 1983). Heterogeneous bioclastic strata (Msto; Fig. 9D), characterised by poorly sorted, matrix-supported, gravel-grade layers of disarticulated bivalve shells and rounded mud balls, are sporadically present interbedded with the blue marls (Mmar). Structureless sandstones (Mstl) are associated with FA7 and are described as fine to very fine calcarenites with irregular and bioturbated bedding surfaces.

Interpretation. The lithofacies of the association record the deposition of fine material in a restricted back-barrier lagoon (Riding & Wright, 1981; Steel *et al.*, 2012). Evidence of conformable superposition of supratidal associations onto the marly facies (Mmar; Fig. 9A) suggests a lagoonal mud depositional setting rather than deposition in deeper water (FA11). Features indicating subaerial exposure in peloidal packstones (Mfen) are interpreted as the expression of localised shallower zones of the lagoon with marginal intertidal properties. Gravel-grade heterogeneous bioclastic strata (Msto) are interpreted as 'spill-over' storm units deposited during high-energy events that locally disrupted deposition of marl in the lagoon (Wilson & Mohrig, 2021). Structureless marine facies (Mstl) are interpreted as the record of diagenetically altered intermittent bedform migration allowing substrate reworking by benthic biota (Melnyk *et al.*, 2025).

Sandy subtidal channel-fill association (FA8)

Description. The sandy subtidal channel-fill association (Fig. 10) is primarily composed of

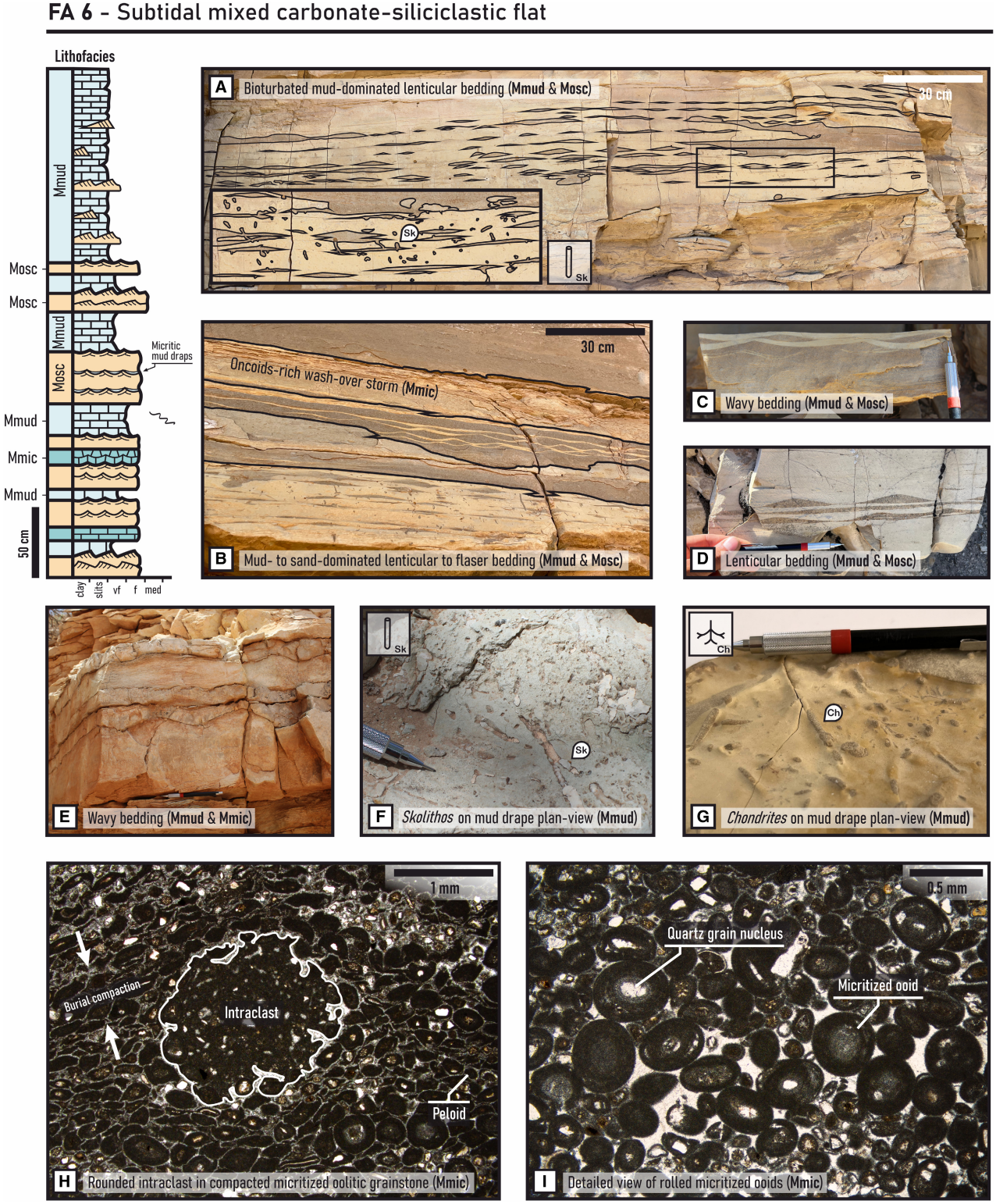

Fig. 8. Lithofacies diversity of subtidal mixed carbonate–siliciclastic flat facies association (FA6). (A to E) Mud-dominated lenticular bedding to sand-dominated flaser bedding (Mmud & Mosc), note the abundant Skolithos burrows in A. (F) Skolithos on Mmud drape plan view. (G) Sandy Chondrites burrow infills on Mmud drape plan view. (H, I) Thin section detail of micritised oolitic grainstones facies (Mmic). The suggested vertical facies distribution represents the idealised sequence of a shallowing upward mixed subtidal flat.

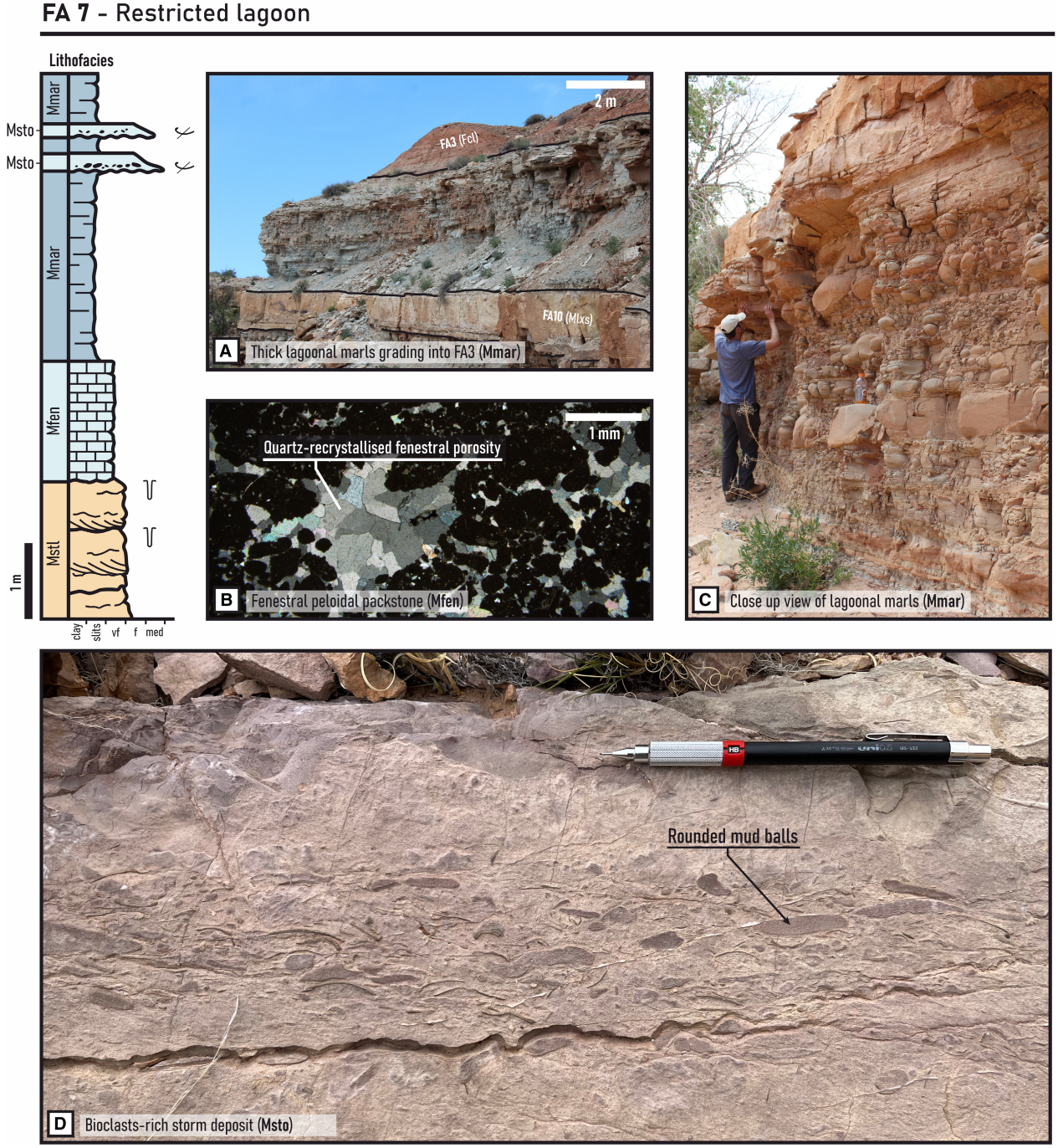

Fig. 9. Lithofacies diversity of restricted lagoon association (FA7). (A, C) Thick lagoonal marl deposits conformably capped by FA3. (B) Thin-section view of fenestral fabric in peloidal packstone facies Mfen. (D) Poorly sorted heterogeneous bioclastic storm deposit (Msto). Note the presence of rounded mud balls. The suggested vertical facies distribution represents a possible succession of restricted lagoonal lithofacies.

strata dominated by indicators of high sediment load deposited under bidirectional currents (lithofacies Mhb and Mstl; Table 2). It is characterised by fine-grained, well-sorted ripple-laminated sandstone (Mhb) sporadically displaying herringbone cross-stratification sets

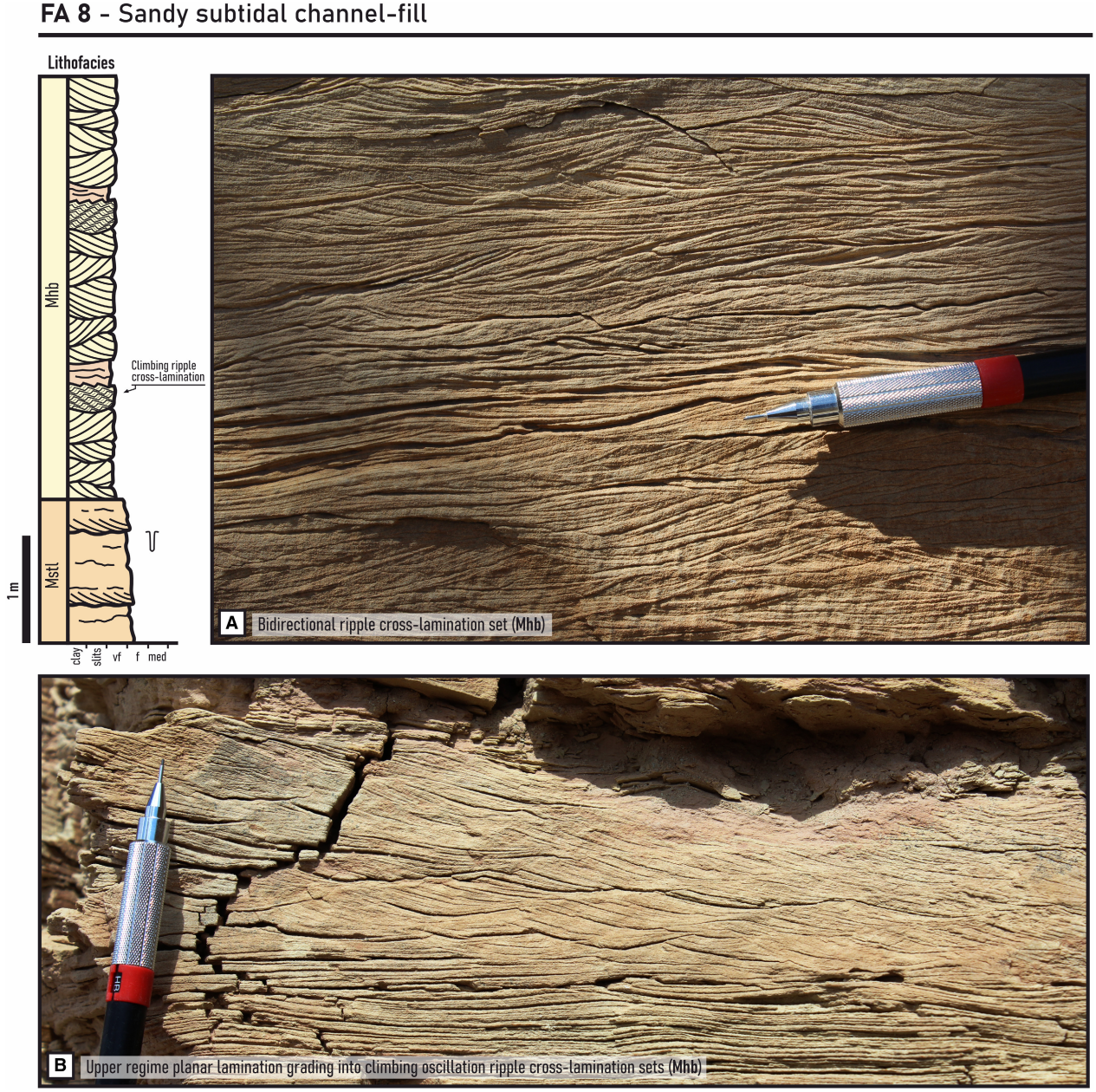

Fig. 10. Lithofacies diversity of sandy subtidal channel-fill association (FA8). (A) Herringbone ripple cross-lamination sets (Mhb). (B) Upper regime planar lamination grading into climbing ripple cross-lamination sets (Mhb). The suggested vertical facies distribution represents the variability of sedimentary structures and lithofacies for a sandy subtidal channel-fill.

(Fig. 10A) and upper flow regime parallel lamination. Oscillatory ripple cross-lamination can be observed aggrading into climbing current ripple cross-lamination sets (Fig. 10B). Structureless marine sandstone (Mstl) with irregular bedding surfaces can be deposited adjacently to ripple-laminated sandstone. Channel fills of the association are typically characterised by fairly planar bedded units, although few examples of decametre-wide erosive lenses that pinch out rapidly have been reported by the present authors in sections not discussed in this study.

Interpretation. The facies of sandy subtidal channel-fill associations record together the migration of sandy bedforms under alternating confined subtidal currents with varying flow directions and velocities (Visser, 1980; Allen & Homewood, 1984). Upper flow regime planar laminations combined with climbing ripple cross-lamination sets (Mhb) suggest sudden increases in sediment load. These features are typically associated with tidal channel fills (e.g. Lanier & Tessier, 1998). Together, the relatively low abundance of sandy subtidal channel-fill associations and their lack of clear erosive surfaces in two-dimensional views are evidence supporting a microtidal regime. This contrasts with other tidal channel fills previously documented in younger meso-tidal strata of the San Rafael Group (Zuchuat *et al.*, 2018).

Marine facies associations

Oolitic tidal dune association (FA9)

Description. The oolitic tidal dune association (Fig. 11) marks deposition in the open-marine facies belt where lithofacies linked to variable processes are combined (Mxs, Mbw, Mhb; Table 2). The association is dominantly composed of laterally extensive, kilometre-scale, superimposed sets of cross-stratified oolitic and bioclastic grainstone (Mxs; Fig. 11A and B). Dune toesets are typically associated with mud drapes and can sporadically display reactivation surfaces. The diverse bioclastic composition of Mxs facies is dominated by coated gastropods, bivalves, bryozoan and crinoidal debris (Cuffey & Ehleiter, 1984; Taylor & Wilson, 1999; Tang *et al.*, 2000) coupled with occasional millimetre-scale intraclasts (Fig. 11C to E). Mxs facies are occasionally associated with herringbone ripple cross-laminated sandstone (Mhb) and low-energy laminated bioclastic wackestone facies (Mbw).

Interpretation. The association records the migration of compound tidal dunes or sand waves (*sensu* Gonzalez & Eberli, 1997) on an oolitic-rich sand shoal (Rankey & Reeder, 2012). The superimposition of oolitic and bioclastic cross-stratified grainstone sets suggests that sediment fluxes are sufficiently high to allow successive bedforms to climb over bigger-scale compound dunes and thus to generate complex sedimentary architectures with surfaces of multiple orders (Olariu *et al.*, 2012). Despite recording one overall unidirectional flow direction dominantly (Fig. 11A), feathering patterns between mud drapes and dune toesets (Fig. 11B) are interpreted as slack tide settlement of fine-grained material during current reversal between ebb and flood flows. Direct tidal influence was occasionally recorded by herringbone ripple cross-laminated sandstone (Mhb) facies. Although resedimented, the high bioclastic content of the association suggests a higher biological activity in this stronger energy setting compared to the tidally dominated environments described previously (FA8 and FA9). Micritic coating of skeletal grains is here associated with a microbial activity (i.e. Védrine *et al.*, 2007). The sporadic transition from oolitic and bioclastic cross-stratified grainstone (Mxs) to bioclastic wackestone (Mbw) is interpreted as the expression of deepening upward successions. This association marks the transition from the subtidal to the open-marine facies belt where deposits are controlled by a combination of tidal and wave processes.

Wave-dominated shoreface to foreshore association (FA10)

Description. The wave-dominated shoreface to foreshore association (Fig. 12) comprises lithofacies associated with sediment deposited by high-energy, subaqueous processes (Mlxs, Mhcs and Mstl; Table 2). It is characterised by laterally continuous decametre-scale units of fine-grained, well-sorted sand. Convex-up hummocky and concave-up swaley cross-stratification sets (Mhcs; Fig. 12C and D) are deposited where flow superimposition is generating complex oscillatory bed shear stress. Low-angle cross-stratification sets (Mlxs; Fig. 12A

Fig. 11. Lithofacies diversity of oolitic tidal bar association (FA9). (A) and (B) Sedimentary architecture of cross-stratified oolitic tidal dune sets (Mxs). Note the superimposition surfaces and the mud drapes on dune toesets. (C) Detailed view of Mxs bioclasts. (D, E) Thin section views of Mxs facies displaying various ratios of oolitic, bioclastic and siliciclastic content. The suggested vertical facies distribution represents the idealised deepening upward sequence of an oolitic tidal bar.

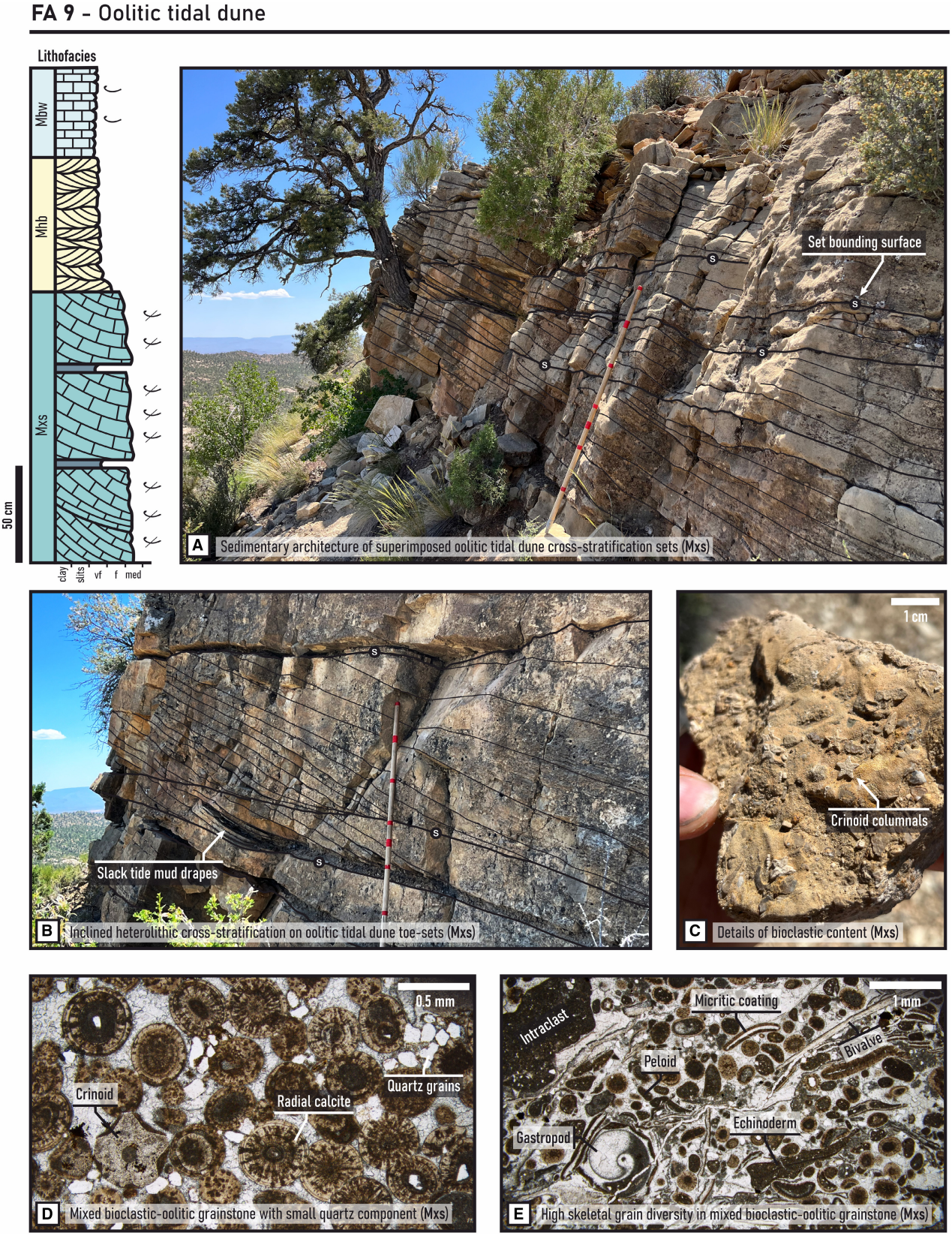

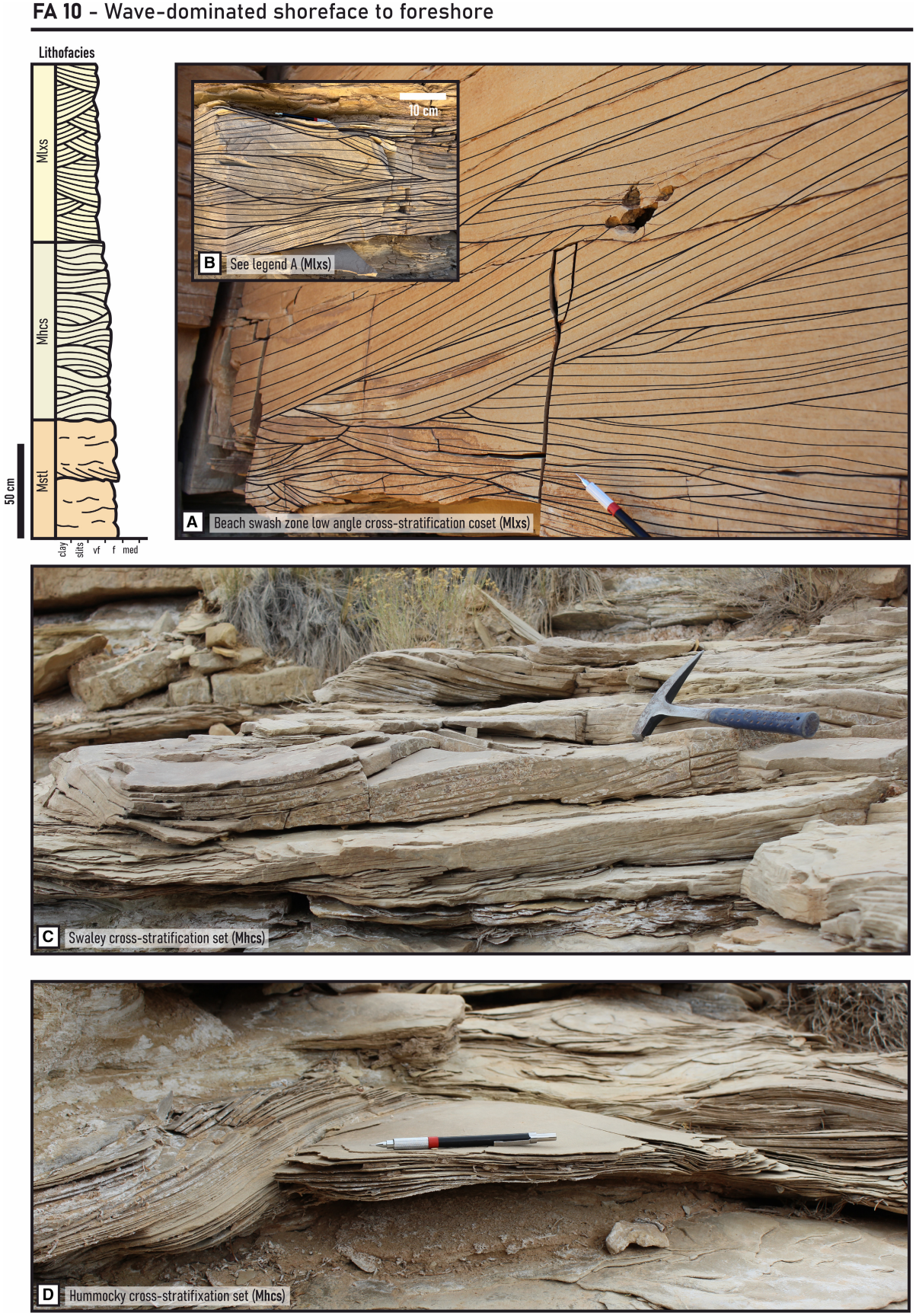

Fig. 12. Lithofacies diversity of wave-dominated shoreface to foreshore association (FA10). (A, B) Low-angle cross-stratification sets (Mlxs) associated with beach swash-zone deposits. (C) Swaley cross-stratification set (Mhcs). (D) Hummocky cross-stratification set (Mhcs). The suggested vertical facies distribution represents the idealised shallowing-upward sequence of a wave-dominated sandy foreshore.

and B), coupled with occasional upper regime parallel laminations and oscillatory ripple cross-laminations, are associated with localised high-energy sediment reworking and short-distance transport. Both hummocky cross-stratification (Mhcs) and low-angle cross-stratified sets (Mlxs) can be observed grading vertically into one another and can be coupled with marine facies Mstl.

Interpretation. These facies record together the progradation of shoreface to foreshore barrier-island successions where wave action was the dominant mechanism (McCubbin, 1982; Dalrymple & Rivers, 2023). Sediment surfaces at depths below the fair-weather base were affected by current superimposition and by sediment mobilisation from regular wave action during storm events that produced hummock and swale bedforms (Mhcs; Duke, 1985; Cheel & Leckie, 1993). Low-angle cross-stratification sets (Mlxs) are associated with much shallower water depths and are interpreted as migration of beach swash zones and associated upper regime parallel laminations are linked to low-tide run-offs.

Offshore transition association (FA11)

Description. The offshore transition association (Fig. 13) marks the open-marine end-member setting of the studied area and is composed of lithofacies Mmud, Mmar, Mbw and Mhg (Table 2). Carbonate facies are dominated by laterally continuous, kilometre-scale, poorly sorted bioclastic grainstone beds with skeletal grains derived from FA9 (Mhg; Fig. 13B). Regionally extensive, highly oxidised hardground surfaces are sporadically present with layers of oriented and disarticulated bivalve shells and brachiopods. Such surfaces are often associated with *in situ* colonies of encrusting *Liostrea strigilecula* growing as ostreoliths over sedimented bioclasts (Wilson & Palmer, 1994; Wilson *et al.*, 1998). Carbonate mudstone (Mmud) and bioclastic wackestone (Mbw) containing skeletal grains include disarticulated bivalve shells (*Plicatula* and *Ostreida*) and brachiopods that are sporadically associated with marly facies (Mmar).

Interpretation. These facies record together the deposition of tempestite beds (Mhg) below the fair-weather wave base in the offshore transition zone (Myrow & Southard, 1996; Rodrigues *et al.*, 2024). In this scenario, intermittent basinward fluxes of oolitic and bioclastic material of the oolitic tidal dune association (FA9) were triggered by storm events and are recorded as strata of poorly sorted resedimented material interbedded with offshore marls (Mmar) and lime mudstones (Mbw). Correlative hardground surfaces are associated with long depositional hiatuses between storm events. Carbonate-rich muddy facies (Mmud and Mbw) are linked to fair-weather deposition along the ramp and may vary in proportions due to localised changes in hydrodynamic processes (Colombié *et al.*, 2025).

STRATIGRAPHIC FRAMEWORK AND GENERALISED MODEL

A reconstruction of the regional stratigraphic framework based on 11 sedimentary logs correlated along a palaeoshoreline-parallel transect (Fig. 2) highlights spatial and temporal variations in the distribution of facies associations (Fig. 14). Vertical evolutions of facies proportions are used to define regressive and transgressive system tracts. Facies dislocations are interpreted as maximum regressive surfaces (MR) and Maximum Flooding Surfaces (MF) which bound transgressive systems tracts and regressive systems tracts (Embry & Johannessen, 1993). Analysis of this framework demonstrates that the shallow-marine system represented by the Carmel Formation preserves the sedimentary record of a mixed arid tidal flat system (Fig. 15) undergoing two T-R sequences in which regressive systems tracts are dominated by aeolian to supratidal deposits and transgressive systems tracts are dominated by intertidal to open-marine deposits. Both spatial and vertical facies distributions within time-equivalent packages demonstrate complex stratigraphic arrangements with numerous transitions between facies associations reflecting a

Fig. 13. Lithofacies diversity of offshore transition facies association (FA11). (A) Sedimentary architecture of alternating marly facies Mmar, distal tempestite shelly beds Mhg and mudstone facies Mmud. (B) Detailed photographs of oxidised hardground surfaces Mhg displaying various bivalves and brachiopod shells. The suggested vertical facies distribution represents the idealised deepening upward sequence within distal basin settings.

combination of depositional processes and sediment types co-occurring within facies belts.

Spatial complexity

As similarly described in the model of Bádenas *et al.* (2018) for mixed carbonate-clastic tidal flats, the tidal succession of the Carmel Formation is characterised by numerous lateral transitions of facies associations within system tracts, thus suggesting a combination of processes and sediment sources across its palaeo-shoreline (Fig. 14). Lateral extrapolation of facies associations within regressive and transgressive

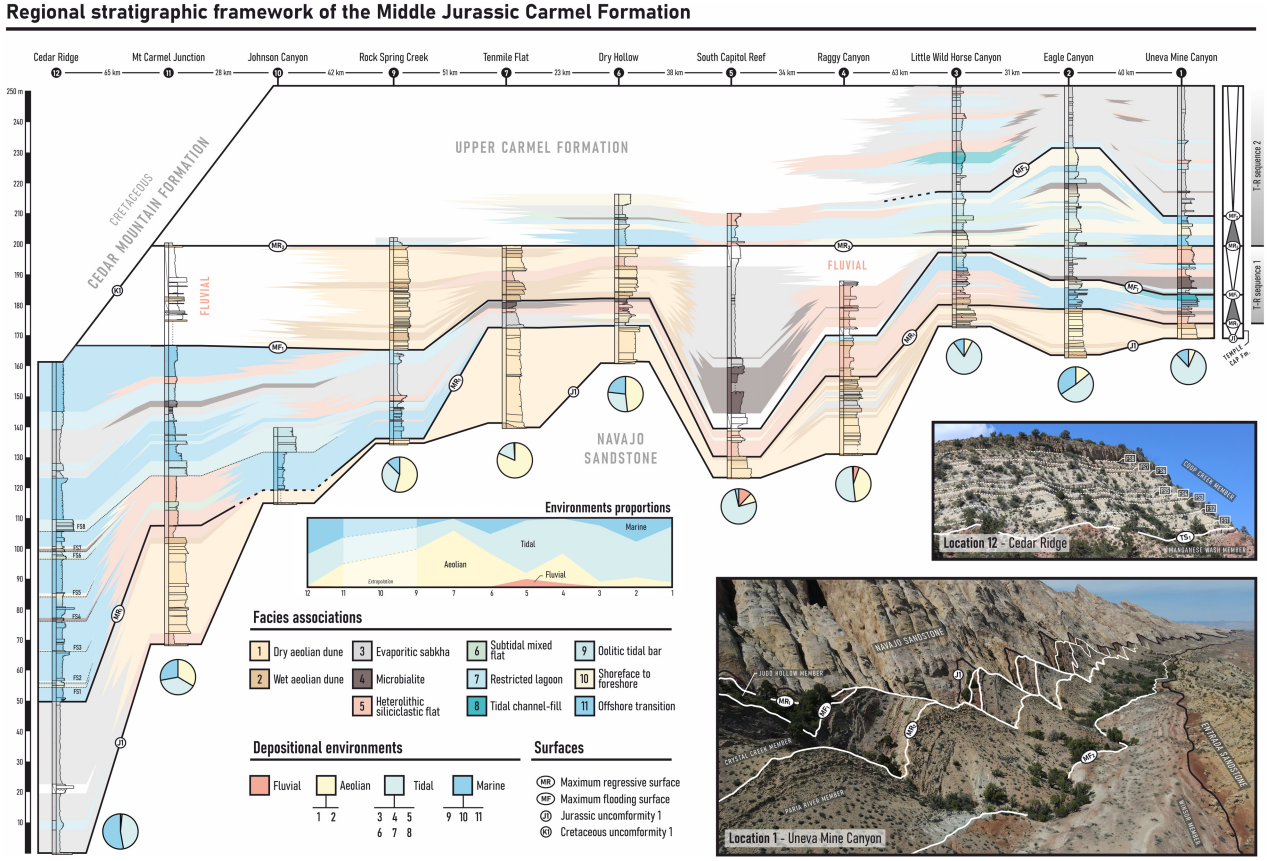

Fig. 14. Regional stratigraphic framework of the Middle Jurassic Carmel Formation. This correlation panel is based on a palaeoshoreline-parallel transect (Fig. 2) depicting the spatio-temporal evolution of facies association distributions within the system tracts of two T-R sequences. Depositional environment proportions of each section are provided. Main correlative surfaces are annotated on outcrop panels for both Sections 1 and 12.

systems tracts of T-R sequences regularly displays discontinuous units. Lateral stratigraphic complexities resulting from this variability are linked to plan-view autocyclic mechanisms and may challenge correlations between sections at the scale of facies associations. Nevertheless, four depositional elements – that combine key co-occurring facies associations and are characterised by their variable proportions – may be defined for specific parts of the system: (i) supratidal to continental transition; (ii) sub- to intertidal transition; (iii) protected subtidal and (iv) wave-dominated subtidal (Fig. 15).

Regressive systems tracts are characterised by a combination of facies associations suggesting transitional settings from supratidal to aeolian facies belts which together define a supratidal to continental transition depositional element (Fig. 15B). In this part of the system, migrating aeolian dunes (FA1) may be affected by tidal reworking (FA2) and may laterally pinch out into evaporitic sabkha deposits (FA3) and ultimately into microbial mats (FA4). Microbialite associations are deposited within very restricted depositional zones where specific hydrodynamic and environmental conditions are favourable for their development. The occurrence of this facies association marks the maximum landward extent of the sub- to intertidal depositional element (Fig. 15A). Localised increases in aeolian facies associations within regressive system tracts (Sections 6 to 9; Fig. 14) are interpreted as dune field encroachment events onto the coastal plains.

Transgressive systems tracts are expressed by different depositional elements based on the position relative to the basin depocentre. The sub- to intertidal transition depositional element

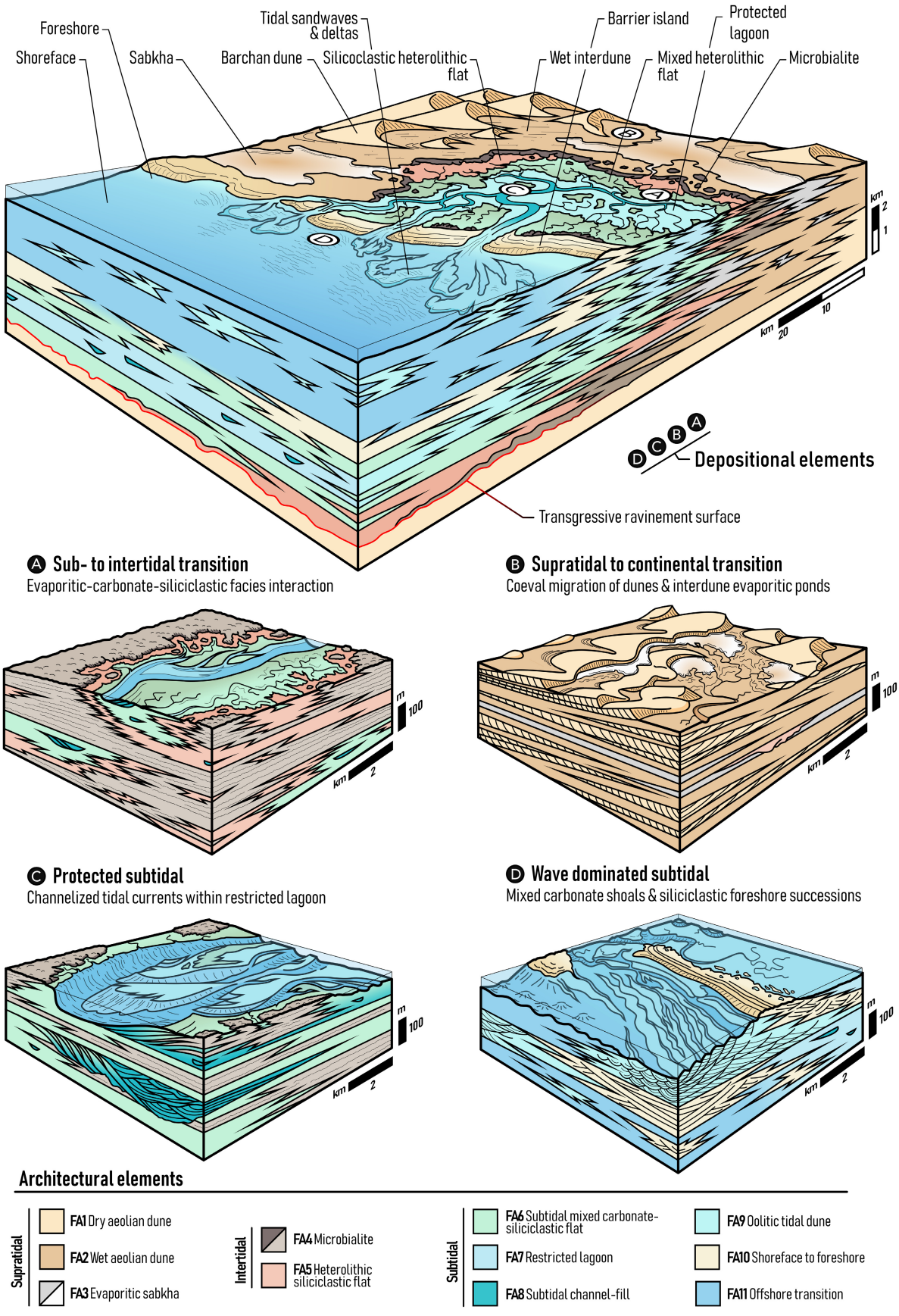

Fig. 15. Integrated dynamic facies model for a mixed siliciclastic-carbonate tidal flat in transgressive systems with detailed depositional element models for (A) sub- to intertidal transitions, (B) supratidal to continental transitions, (C) protected subtidal and (D) wave-dominated subtidal sub-environments.

(Fig. 15A) is defined by the co-occurrence of microbialite associations (FA4), heterolithic siliciclastic intertidal flat (FA5) and subtidal mixed siliciclastic-carbonate flat (FA6). Lateral transitions between these associations are gradual and follow an increase in average water depth between high and low tides. The protected subtidal depositional element (Fig. 15C) is defined by the presence of sporadic sandy channel fills (FA8) within restricted lagoon deposits (FA7). Finally, the wave-dominated subtidal depositional element (Fig. 15D) is defined by coeval depositions of open-marine facies associations (FA9–FA11) that may grade into restricted lagoon associations (FA7) due to coastline migration or shoreface sediment routing. Overall higher proportions of wave-dominated subtidal depositional elements within transgressive systems tracts (Sections 10 to 12; Fig. 14) reflect the influence of basinward increase in accommodation. Parasequence-like successions may be observed in such a distal-most depositional element. Eight flooding surfaces (FS1–FS8) that are partly equivalent to the sequence boundaries of Blakey *et al.* (1996) are defined, where carbonate ramp deposition is dominant (Section 12; Fig. 14). However, landward correlation of these parasequences is challenged by their amalgamation in proximal parts of the system. In continental parts of the system (Sections 1 to 7; Fig. 14), transgressive system tracts are either condensed into aeolian deflationary super surfaces (Havholm & Kocurek, 1994) or expressed as protected subtidal and sub- to intertidal transition depositional elements.

Together, these depositional elements can be placed in the broader context of a mixed siliciclastic-carbonate tidal flat undergoing periods of aeolian dune field encroachment (RST) and periods of deflation triggered by tidal embayments (TST) (Fig. 15). Analysis of the presented stratigraphic framework suggests that correlation of mixed paralic deposits is challenging at the association scale as high lateral facies variabilities will tend to generate unpredictable complexities of architecture. It is, however, possible to define generic models at the depositional element scale within the T-R sequence framework and, ultimately, to correlate transgressive and regressive system tracts at a basin scale.

Temporal evolution

Analysis of the vertical stratal evolution of the Carmel Formation reveals two major transgressive-regressive (T-R) sequences bounded by maximum regressive surfaces (MR1 & MR2; Fig. 14) which, together with associated maximum flooding surfaces (MF1 & MF2), define the current lithostratigraphic subdivision (Fig. 1). Both T-R sequences record gradual tidal flat fluctuations across the coastal plains with transgressive system tracts characterised by marine- to intertidal-dominated successions and regressive system tracts associated with supratidal evaporites and aeolian deposits. Vertical shallowing-up trends in facies associations may be observed locally within system tracts and are interpreted as the expression of internal process variability within tidal belts.

Following a significant hiatus recorded during the termination and erosion of the Navajo Sandstone erg (J-1 unconformity), early stages in the erg development of the Temple Cap Formation were recorded in variable thicknesses as palaeolow infills and are equivalent to the lower aeolian sequences of the Page Sandstone (Dickinson *et al.*, 2010; Doelling *et al.*, 2013). The preservation of this primary depositional stage reflects the return of positive accommodation and sediment availability on the Colorado Plateau after a significant period of uplift during the late Glen Canyon Group times (Marzolf, 1991; Bromley, 1992).

Where preserved, the Temple Cap Formation is capped by a deflationary supersurface (MR1; Fig. 14) marking the initiation of the first major transgression of the Carmel Formation (T-R sequence 1), although older supratidal facies that were deposited prior to MR1 can be observed in the Saint George area (Manganese Wash Member). Open-marine carbonate ramp (Co-op Creek Limestone) to mixed tidal flat

associations (Judd Hollow Member) are dominant in the TST of T-R sequence 1, but thin eastward (Fig. 14). Correlative hardgrounds in the offshore transition association (FA11; Fig. 13) at the base of this TST in the distal settings can be traced out across several sections in the San Rafael Swell region (Sections 1 to 3; Fig. 14).

The following RST in the T-R sequence 1 is marked by the encroachment of the Page Sandstone erg onto the coastal plains of the Sundance Sea. Vertical facies dislocations from marine and tidal facies associations into the younger aeolian strata are used to define a maximum flooding surface (MF1; Fig. 14). Tidally reworked aeolian associations FA2 are dominant in Sections 6 to 9 (Thousand Pockets Member) and grade both westward into terminal distributary fluvial system successions and eastward into supratidal evaporitic successions (Crystal Creek Member). An increase in wave action is observed in the preserved TST of T-R sequence 2, which caps the underlying aeolian strata (Paria River Member). Vertical facies transitions to the following and final RST are gradational and demonstrate an overall retreat of the Sundance Sea. Studied sections covering the T-R sequence 2 (Sections 1 to 3; Fig. 14) demonstrate a regional decrease in continental sediment availability as regressive-stage aeolian deposits are replaced by terminal fluvial fan facies not discussed in this study (Jones & Blakey, 1997).

DISCUSSION: STRATAL DISORDER AND FACIES MOSAIC

Markov chain analysis

The presented facies analysis of peritidal successions in the sediments of the Carmel Formation demonstrates that correlation between the studied sections at the facies association scale is very challenging. Successions within system tracts often do not match those in neighbouring logs, which suggests that, at this scale, observable vertical trends in facies associations may be artefacts only, controlled principally by autogenic mechanisms. To evaluate this, numerical techniques based upon Markov analysis (Burgess, 2016) have been applied to three tidally dominated sections of the Carmel Formation (sections 1 to 3, Fig. 16) in order to quantify their degree of order at both lithofacies and facies association scales. Transition probability matrices demonstrate that several transitions between facies and facies associations are more likely to occur in these three sections. This result may be biased by the large number of potential transitions that could theoretically happen but are not recorded in these specific cases. Lithofacies and facies association Markov numbers of each section are given in relation to the density profiles of their corresponding randomly shuffled successions. Results demonstrate that each observed succession may be classified as statistically disordered at both facies and association scales. With the exception of marginal results in Section 2 at the lithofacies scale, all calculated Markov numbers fall below the uppermost 5% threshold defining statistical order. This reinforces the interpretation that (i) observed vertical trends are only apparent products and that (ii) allocyclic parasequence signals in tidally dominated successions may be overprinted by autogenic dynamics (c.f. Zuchuat *et al.*, 2019).

Recent advances (Manifold *et al.*, 2020; Geyman *et al.*, 2021), building upon previous statistical methodologies (Wilkinson *et al.*, 1996, 1997), demonstrate that the stratigraphic record of shallow-marine carbonate can be more challenging to analyse than other systems. Facies mosaic distribution is commonly used to describe modern carbonate systems and is thought to have a high influence on the order of vertical facies successions (e.g. Rankey, 2016). The co-occurrence of different contemporaneous facies associations deposited within system tracts of the Carmel Formation reflects the complex facies mosaic distribution of supra- to subtidal depositional elements. By illustrating process interactions and the plan view distribution of their sedimentary products, the analysis of facies distribution in analogous modern

Fig. 16. Markov chain analysis applied for the tidal succession of Sections 1 to 3. Transverse Probability Matrix and Kernel density distributions are calculated for both lithofacies and facies association datasets. Results show Markov numbers below the range of statistically relevant ordered successions (upper 5%) for both lithofacies and facies association datasets. Method adapted from Burgess (2016).

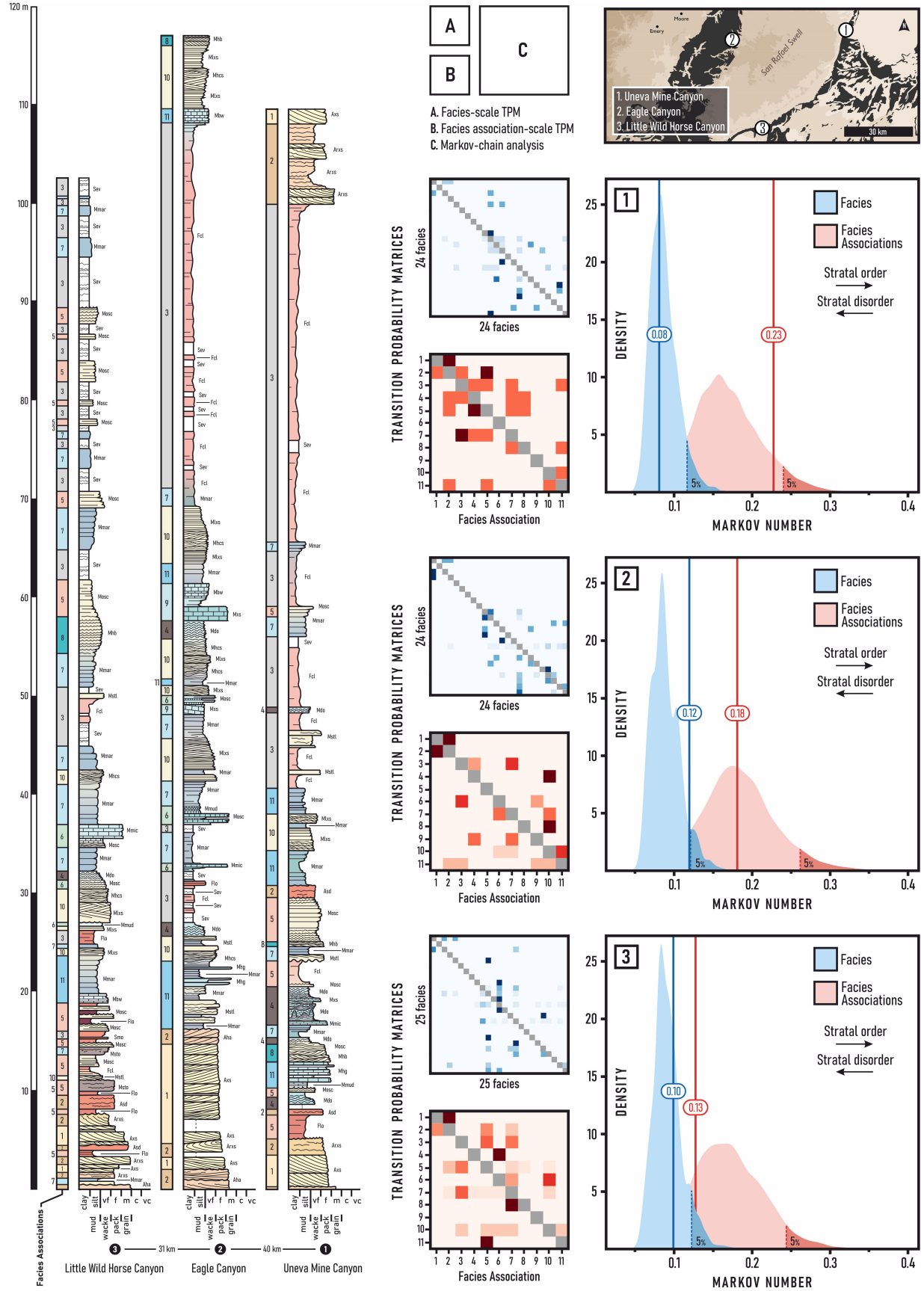

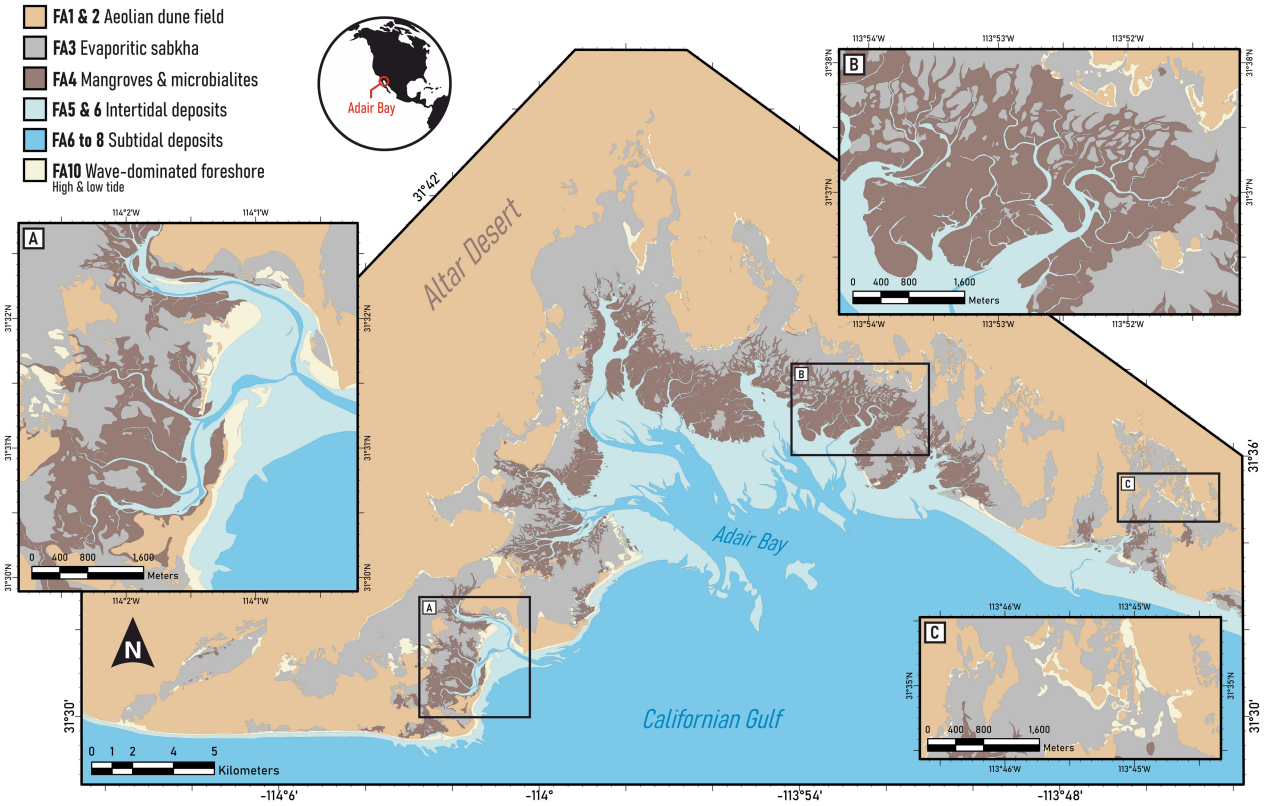

Fig. 17. Sedimentary facies distribution map of Adair Bay, Mexico. Interpreted facies associations are adapted from the discussed Carmel Formation facies scheme and have been manually drawn over satellite views from the ESRI World Imagery data bank.

systems can constrain the autocyclic controls over the spatio-temporal complexity of system tracts observed in the Carmel Formation.

Facies mosaic in modern analogous systems

The Adair Bay in Mexico (Fig. 17) is a complex tidal embayment bordering a coastal desert (Ives, 1949; Beveridge *et al.*, 2006) and presents similarities with palaeoenvironmental interpretations of the Carmel Formation. The application of the presented facies scheme to high-resolution satellite images reveals an overall segregation between the main facies belts of the Adair Bay over kilometres: (i) aeolian dune field (FA1 and FA2); (ii) evaporitic sabkha (FA3); (iii) mangroves and microbialites (FA4); (iv) intertidal deposits (FA5 and FA6); (v) subtidal deposits (FA7 and FA8) and (vi) wave-dominated foreshore (FA10). However, spatial transitions between facies associations are more erratic at a smaller, sub-kilometre scale. Foreshore deposits are occasionally truncated by smaller tidal inlets and show preferential orientations in response to wave action (Fig. 17A). The facies belt delimitation between sabkha ponds and microbialites deposits is hard to evaluate as both facies associations may be deposited concomitantly within the same relative bathymetric zone (Fig. 17B). Furthermore, the distribution of intertidal deposits seems to be governed by channel avulsion due to the degree of channel sinuosity which, in itself, adds spatial complexity to this transitional facies belt. Finally, dune field-sabkha interactions reveal a discontinuous and scattered distribution of both facies associations (Fig. 17C). Facies belts of the Adair Bay are reasonably defined at a regional scale but sediments are erratically distributed in a mosaic of facies associations at the local scale. As supported by the presented Markov chain analysis, a non-cyclic and unpredictable stratigraphic record will arise from such a randomised plan view facies distribution. This finding

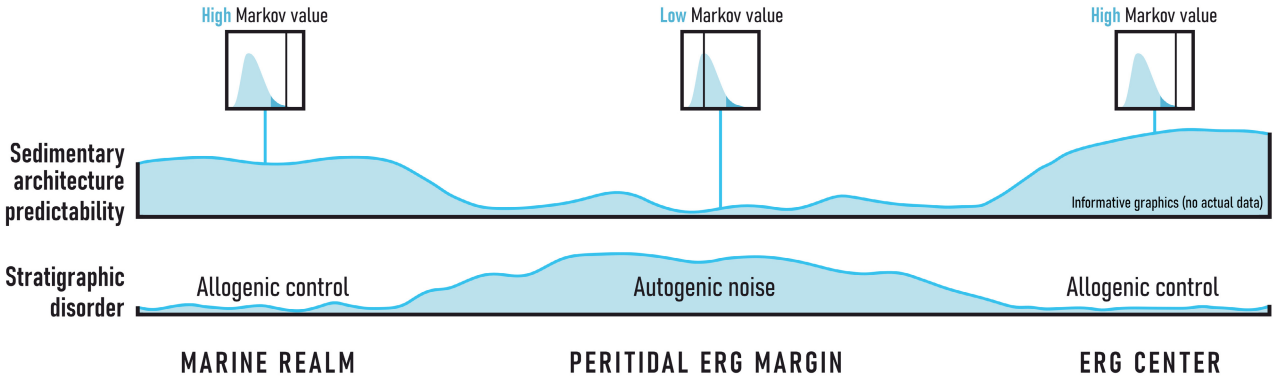

Fig. 18. Informative graphics illustrating the increasing stratigraphic disorder across peritidal transitional zones between aeolian and marine environments and direct implications for sedimentary architecture predictability.

contrasts with recent studies demonstrating clear evidence of allocyclic signals in ancient peritidal deposits (e.g. Spalluto *et al.*, 2024; Read *et al.*, 2025). As demonstrated by the difficulties in correlating marine parasequences landward (Section 12; Fig. 14), autogenic phenomena specific to restricted coastal settings and influenced by coastal palaeomorphology have the potential to inhibit the expression of larger-scale controlling factors and the preservation of their signature in the rock record (Alsharhan & Kendall, 2003; Zhong *et al.*, 2023; Zuchuat *et al.*, 2023). In such scenarios, stratigraphic arrangements and three-dimensional distributions of sedimentary architectures may be unpredictable parameters (Fig. 18).

Controlling factors on sedimentary evolution

Facies dislocations used to correlate sequence-stratigraphic surfaces between system tracts of the Carmel Formation are interpreted as the result of larger-scale allocyclic forcing. Discussion of the overarching mechanism(s) controlling the relative sea-level fluctuations observed in this Bajocian system is still open. Recent isotopic analysis suggests a geochemical decoupling between the restricted Sundance Sea and the Jurassic open water masses (Danise *et al.*, 2020), negating the idea of a eustatic control. Instead, the vertical facies evolution of the Carmel Formation could be explained by regional tectonic bulging events related to Jurassic cordilleran arc tectonism (Bjerrum & Dorsey, 1995). In addition to directly affecting accommodation and base levels within the Utah-Idaho Trough, regional bulging may have had an indirect influence on aeolian sediment availability and upon the dune field encroachment stages. Conversely, cyclicity has been demonstrated in the coaeval aeolian succession of the Page Sandstone, Arizona, suggesting a strong water table control over the preservation of these coastal aeolian strata (Kocurek *et al.*, 2001). Locally, observed thicknesses vary drastically over the studied transect (Fig. 14) and are thought to be influenced by spatial changes in palaeotopography and localised accommodation. Differential subsidence is now broadly recognised as a potential controlling factor on sediment distributions in tidally influenced systems (e.g., Smyrak-Sikora *et al.*, 2020). The combined effects of such controls may have an influence on the nature of the preserved strata that is not considered here.

Comprehensive models accounting for spatial arrangement and morphological complexities of arid peritidal environments are numerous and provide tools to elucidate the controls on facies distribution for different relative sea levels. The development of tidal paralic systems along arid coastlines is often associated with complex interactions between processes that lead to the coeval deposition of siliciclastic, carbonate and evaporitic sediments in restricted environments (Lokier *et al.*, 2013; Billeaud *et al.*, 2014; Rivers *et al.*, 2020). In such scenarios, the spatial distribution of sediment is grossly governed by energy levels and relative abundances of tide and wave processes, and mixed tidal environments are usually described by well-defined facies belts: (1) supratidal sabkha successions irregularly supplied with terrigenous material; (2) mixed

intertidal zones occasionally disrupted by storms and (3) subtidal carbonate ramp with occasional lateral facies transitions to wave-dominated siliciclastic shoreface units (e.g. Alsharhan & Kendall, 2003). Other models for ancient shallow carbonate ramp systems incorporate the idea of facies mosaic distribution to justify high lateral facies heterogeneities (Bádenas *et al.*, 2010, 2018; Sequero *et al.*, 2018). Despite this, no generic model unifies plan-view complexities, recorded sedimentary architectures and inherent stratigraphic heterogeneities arising from facies mosaic distributions. The model proposed in this study is the first qualitative integrated dynamic facies model for mixed carbonate–siliciclastic arid tidal flats. It encapsulates stochastic facies transitions within depositional elements and their stratigraphic arrangement within system tracts.

CONCLUSION

Tidal flat depositional systems developing under arid conditions are the scene of intricate interactions between competing depositional processes and involve an intricate mixing of multiple sediment fractions. This analysis captures the spatio-temporal facies variability of a mixed transitional paralic system in regard to preserved lithologies (evaporites, terrigenous clastics and carbonates) and to sedimentary processes (aeolian, tides and wave action) occurring concurrently within different facies belts.

Complex lateral facies transitions are characteristic of such systems and may challenge correlations over long distances. Stratigraphic successions will tend to display disordered stratal arrangements within system tracts at the facies and association scale. Stochastic organisation of facies mosaics is presumed to be the driving mechanism of architectural disorder in tidal stratigraphic distribution, and we suggest that the record of dynamic facies mosaic distribution over time may overprint allocyclic signals at such scale.

Arid paralic successions are often treated as a whole for assessing stratigraphic sealing at reservoir margins. The work presented here suggests that the resolution at which these margins are evaluated should be refined in order to capture the facies diversity and stratigraphic complexity within system tract packages at depositional-element scale, and it offers a generic model at this scale. Such systems may be subdivided into separate depositional elements defined by differences in facies proportions linked to changes in depositional processes and energy levels across their margins, within a transgressive-regressive framework. Stratal disorder and unpredictable vertical facies successions may challenge sequence-stratigraphic analysis at the association scale. However, the proposed model suggests that recognition of spatio-temporal patterns and correlations at the scale of depositional elements is possible within system tracts.

Incorporating this singular characteristic may help constrain the predictions of reservoir heterogeneities in analogous subsurface successions. Nevertheless, subsurface fluid migration pathways may be deterministically unpredictable below depositional element scale, and this critical uncertainty should be accounted for stochastically in the appraisal carbon storage projects.

ACKNOWLEDGMENTS

This research was conducted during a PhD study undertaken as part of the Centre of Doctoral Training (CDT) in Geoscience and the Low Carbon Energy Transition (GeoNetZero). It is sponsored by Keele University and NeoEnergy Upstream, whose support is gratefully acknowledged. We are also grateful to the United States National Park Service for permitting this research and granting a scientific research permit for Dinosaur National Monument. Oliver Button and Andrew Mitten are acknowledged for providing valuable field support and assisting with observations and interpretations. Reviewers Beatriz Bádenas and Marcos Aurell are gratefully acknowledged for their constructive suggestions and comments. The authors declare that they have no conflict of interests.

DATA AVAILABILITY STATEMENT

The data that support the findings of this study are available from the corresponding author upon reasonable request.

REFERENCES

Ainsworth, R.B. (2010) Prediction of stratigraphic compartmentalization in marginal marine reservoirs. *Geol. Soc. London Spec. Publ.*, **347**, 199–218.

Ainsworth, R.B., **Vakarelov, B.K.** and **Nanson, R.A.** (2011) Dynamic spatial and temporal prediction of changes in depositional processes on clastic shorelines: toward improved subsurface uncertainty reduction and management. *AAPG Bull.*, **95**, 267–297.

Allen, P.A. and **Homewood, P.** (1984) Evolution and mechanics of a Miocene tidal sandwave. *Sedimentology*, **31**, 63–81.

Alsharhan, A.S. and **Kendall, C.S.C.** (2003) Holocene coastal carbonates and evaporites of the southern Arabian Gulf and their ancient analogues. *Earth Sci. Rev.*, **61**, 191–243.

Anderson, P.B., **Willis, G.C.**, **Chidsey, T.C.** and **Sprinkel, D.A.** (2024) Geology of Glen Canyon National Recreation Area, Utah-Arizona. In: *Geology of Utah's Parks and Monuments* (Eds Sprinkel, D.A., Chidsey, T.C., Jr., Anderson, P.B. and Wills, G.C.), Vol. **28**, pp. 391–433. Utah Geological Association Publication, Salt Lake City.

Andreason, M.W. (1992) Coastal siliciclastic sabkhas and related evaporative environments of the Permian Yates formation, North Ward-Estes Field, Ward County, Texas. *AAPG Bull.*, **76**, 1735–1759.

Bádenas, B., **Aurell, M.** and **Bosence, D.** (2010) Continuity and facies heterogeneities of shallow carbonate ramp cycles (Sinemurian, Lower Jurassic, North-East Spain): heterogeneities in Sinemurian carbonate cycles. *Sedimentology*, **57**, 1021–1048.

Bádenas, B., **Aurell, M.** and **Gasca, J.M.** (2018) Facies model of a mixed clastic–carbonate, wave-dominated open-coast tidal flat (Tithonian–Berriasian, north-east Spain). *Sedimentology*, **65**, 1631–1666.

Beveridge, C., **Kocurek, G.**, **Ewing, R.C.**, **Lancaster, N.**, **Morthekai, P.**, **Singhvi, A.K.** and **Mahan, S.A.** (2006) Development of spatially diverse and complex dune-field patterns: gran Desierto Dune Field, Sonora, Mexico. *Sedimentology*, **53**, 1391–1409.

Billeaud, I., **Caline, B.**, **Livas, B.**, **Tessier, B.**, **Davaud, E.**, **Frebourg, G.**, **Hasler, C.-A.**, **Laurier, D.** and **Pabian-Goyheneche, C.** (2014) The carbonate-evaporite lagoon of Al Dakhirah (Qatar): an example of a modern depositional model controlled by longshore transport. *Geol. Soc. London Spec. Publ.*, **388**, 561–587.

Bilodeau, W.L. (1986) The Mesozoic Mogollon Highlands, Arizona: an early cretaceous rift shoulder. *J. Geol.*, **94**, 724–735.

Bjerrum, C.J. and **Dorsey, R.J.** (1995) Tectonic controls on deposition of Middle Jurassic strata in a retroarc foreland basin, Utah-Idaho trough, western interior, United States. *Tectonics*, **14**, 962–978.

Blakey, R.C. (2014) Paleogeography and paleotectonics of the western interior seaway, Jurassic-Cretaceous of North America. *Search Discov.*, **72**, 30392.

Blakey, R.C. and **Middleton, L.T.** (1983) Permian shoreline eolian complex in central Arizona: dune changes in response to cyclic sealevel changes. *Dev. Sedimentol.*, **38**, 551–581.

Blakey, R.C., **Peterson, F.**, **Caputo, M.V.**, **Geesaman, R.C.** and **Voorhees, B.J.** (1983) Paleogeography of Middle Jurassic continental, shoreline, and shallow marine sedimentation, southern Utah. *Rocky Mountain Section (SEPM)*.

Blakey, R.C., **Peterson, F.** and **Kocurek, G.** (1988) Synthesis of late Paleozoic and Mesozoic eolian deposits of the Western Interior of the United States. *Sed. Geol.*, **56**, 3–125.

Blakey, R.C., **Havholm, K.G.** and **Jones, L.S.** (1996) Stratigraphic analysis of eolian interactions with marine and fluvial deposits, Middle Jurassic Page Sandstone and Carmel Formation, Colorado Plateau, USA. *J. Sed. Res.*, **66**, 324–342.

Bourillot, R., **Vennin, E.**, **Rouchy, J.-M.**, **Durlet, C.**, **Rommevaux, V.**, **Kolodka, C.** and **Knap, F.** (2010) Structure and evolution of a Messinian mixed carbonate-siliciclastic platform: the role of evaporites (Sorbas Basin, South-East Spain). *Sedimentology*, **57**, 477–512.

Breda, A. and **Preto, N.** (2011) Anatomy of an Upper Triassic continental to marginal-marine system: the mixed siliciclastic–carbonate Travenanzes Formation (Dolomites, Northern Italy). *Sedimentology*, **58**, 1613–1647.

Bromley, M. (1992) Topographic inversion of early interdune deposits, Navajo Sandstone (Lower Jurassic), Colorado Plateau, USA. *Sed. Geol.*, **80**, 1–25.

Burgess, P.M. (2006) The signal and the noise: forward modeling of allocyclic and autocyclic processes influencing peritidal carbonate stacking patterns. *J. Sed. Res.*, **76**, 962–977.

Burgess, P.M. (2016) Identifying ordered strata: evidence, methods, and meaning. *J. Sed. Res.*, **86**, 148–167.

Cardenas, B.T., **Kocurek, G.**, **Mohrig, D.**, **Swanson, T.**, **Hughes, C.M.** and **Brothers, S.C.** (2019) Preservation of autogenic processes and allogenic forcings in set-scale aeolian architecture II: the scour-and-fill dominated Jurassic Page Sandstone, Arizona, USA. *J. Sed. Res.*, **89**, 741–760.

Chakrabarti, A. (2005) Sedimentary structures of tidal flats: a journey from coast to inner estuarine region of eastern India. *J. Earth. Syst. Sci.*, **114**, 353–368.

Chan, M.A. (1989) Erg margin of the Permian White Rim Sandstone, SE Utah. *Sedimentology*, **36**, 235–251.

Chapman, M.G. (1989) Implications of rhyolitic ignimbrite boulders in the Middle Jurassic Carmel Formation of southern Utah. *Geology*, **17**, 281–284.

Cheel, R.J. and **Leckie, D.A.** (1993) Hummocky cross-stratification. *Sed. Rev.*, **1**, 103–122.

Chiarella, D. and **Longhitano, S.G.** (2012) Distinguishing depositional environments in shallow-water mixed, bio-siliciclastic deposits on the basis of the degree of heterolithic segregation (Gelasian, southern Italy). *J. Sed. Res.*, **82**, 969–990.

Chiarella, D., **Longhitano, S.G.** and **Tropeano, M.** (2017) Types of mixing and heterogeneities in siliciclastic-carbonate sediments. *Mar. Petrol. Geol.*, **88**, 617–627.

Chiarella, D., **Longhitano, S.G.**, **Spalluto, L.** and **Martinius, A.W.** (2024) Hierarchies of stratigraphic discontinuity surfaces in siliciclastic, carbonate and mixed siliciclastic-bioclastic tidalites: implications for fluid migration in reservoir quality assessment. *Depos. Rec.*, **11**, dep2.307.

Clement, A.M. and **Holland, S.M.** (2016) Sequence stratigraphic context of extensive basin-margin evaporites: middle Jurassic Gypsum Spring Formation, Wyoming, USA. *J. Sed. Res.*, **86**, 965–981.

Cloyd, K.C., **Demicco, R.V.** and **Spencer, R.J.** (1990) Tidal channel, levee, and crevasse-splay deposits from a Cambrian tidal channel system; a new mechanism to produce shallowing-upward sequences. *J. Sed. Res.*, **60**, 73–83.

Colombié, C., **Giraud, F.**, **Guenser, P.** and **Carcel, D.** (2025) Factors controlling carbonate mud production and accumulation on Upper Jurassic western European mixed

siliciclastic–carbonate ramps. *Sedimentology*, **72**, 1963–1991.

Court, W.M., **Paul, A.** and **Lokier, S.W.** (2017) The preservation potential of environmentally diagnostic sedimentary structures from a coastal sabkha. *Mar. Geol.*, **386**, 1–18.

Crabaugh, M. and **Kocurek, G.** (1993) Entrada Sandstone: an example of a wet Aeolian system. *Geol. Soc. London Spec. Publ.*, **72**, 103–126.

Cross, S., **Pettigrew, R.P.**, **Priddy, C.L.**, **Zuchuat, V.**, **Dodd, T.J.H.**, **Mitten, A.J.** and **Clarke, S.M.** (2023) The sedimentological expression of transgression–regression cycles upon Aeolian–marine margins. *Depos. Rec.*, **9**, 335–362.

Cuffey, R.J. and **Ehleiter, J.E.** (1984) New bryozoan species from the Mid-Jurassic Twin Creek and Carmel formations of Wyoming and Utah. *J. Paleontol.*, **58**, 668–682.

Dalrymple, R.W. and **Rivers, J.M.** (2023) A new look at modern carbonate shoals and coastal barrier systems. *Earth-Sci. Rev.*, **246**, 104553.

Dalrymple, R.W., **Zaitlin, B.A.** and **Boyd, R.** (1992) Estuarine facies models; conceptual basis and stratigraphic implications. *J. Sed. Res.*, **62**, 1130–1146.

Danise, S. and **Holland, S.M.** (2017) Faunal response to sea-level and climate change in a short-lived seaway: Jurassic of the Western Interior, USA. *Palaeontology*, **60**, 213–232.

Danise, S., **Price, G.D.**, **Alberti, M.** and **Holland, S.M.** (2020) Isotopic evidence for partial geochemical decoupling between a Jurassic epicontinental sea and the open ocean. *Gondwana Res.*, **82**, 97–107.

De Gibert, J.M. and **Ekdale, A.A.** (1999) Trace fossil assemblages reflecting stressed environments in the Middle Jurassic Carmel Seaway of central Utah. *J. Paleontol.*, **73**, 711–720.

De Gibert, J.M. and **Ekdale, A.A.** (2002) Ichnology of a restricted epicontinental sea, Arapien Shale, Middle Jurassic, Utah, USA. *Palaeogeogr. Palaeoclimatol. Palaeoecol.*, **183**, 275–286.

Demicco, R.V. (1983) Wavy and lenticular-bedded carbonate ribbon rocks of the Upper Cambrian Conococheague Limestone, central Appalachians. *J. Sed. Res.*, **53**, 1121–1132.

Demicco, R.V. (1985) Platform and off-platform carbonates of the Upper Cambrian of western Maryland, U.S.A. *Sedimentology*, **32**, 1–22.

Dickinson, W.R., **Stair, K.N.**, **Gehrels, G.E.**, **Peters, L.**, **Kowallis, B.J.**, **Blakey, R.C.**, **Amar, J.R.** and **Greenhalgh, B.W.** (2010) U-Pb and^{40} Ar/^{39} Ar ages for a Tephra Lens in the Middle Jurassic Page Sandstone: first direct isotopic dating of a Mesozoic Eolianite on the Colorado Plateau. *J. Geol.*, **118**, 215–221.

Doelling, H.H., **Sprinkel, D.A.**, **Kowallis, B.J.**, **Kuehne, P.A.**, **Morris, T.H.** and **Ressetar, R.** (2013) Temple Cap and Carmel Formations in the Henry Mountains Basin, Wayne and Garfield Counties, Utah. In: *The San Rafael Swell and Henry Mountains Basin—Geologic Centerpiece of Utah* (Eds Morris, T.H. and Ressetar, R.), Vol. **42**, pp. 279–318. Utah Geological Association Publication, Salt Lake City.

Duke, W.L. (1985) Hummocky cross-stratification, tropical hurricanes, and intense winter storms. *Sedimentology*, **32**, 167–194.

Einsele, G. and **Ricken, W.** (1991) Limestone-marl alternation-an overview. In: *Cycles and events in stratigraphy* (Eds Einsele, G., Ricken, W. and Seilacher, A.), pp. 23–47. Springer-Verlag, Berlin, Heidelberg.

Embry, A.F. and **Johannessen, E.P.** (1993) *T–R Sequence Stratigraphy, Facies Analysis and Reservoir Distribution in the Uppermost Triassic–Lower Jurassic Succession, Western Sverdrup Basin, Arctic Canada*, Vol. **2**, pp. 121–146. Norwegian Petroleum Society Special Publications, Elsevier, The Netherlands.

Eriksson, K.A. and **Truswell, J.F.** (1974) Tidal flat associations from a Lower Proterozoic carbonate sequence in South Africa. *Sedimentology*, **21**, 293–309.

Evans, G. (1966) A discussion concerning the floor of the northwest Indian Ocean – The recent sedimentary facies of the Persian Gulf region. *Phil. Trans. R. Soc. London A.*, **259**, 291–298.

Ferronatto, J.P.F., **dos Santos Scherer, C.M.**, **Angonese, B.S.**, **Rodrigues, A.G.**, **de Souza, E.G.**, **Kifumbi, C.**, **dos Reis, A.D.**, **Guadagnin, F.** and **Cazarin, C.L.** (2024) Mesoproterozoic siliciclastic stromatolites of Chapada Diamantina (Brazil): morphological types, genesis and environmental context. *J. S. Am. Earth Sci.*, **146**, 105052.

Fryberger, S.G., **Al-Sari, A.M.** and **Clisham, T.J.** (1983) Eolian dune, interdune, sand sheet, and siliciclastic sabkha sediments of an offshore prograding sand sea, Dhahran area, Saudi Arabia. *AAPG Bull.*, **67**, 280–312.

Fryberger, S.G., **Krystinik, L.F.** and **Schenk, C.J.** (1990) Tidally flooded back-barrier dunefield, Guerrero Negro area, Baja California, Mexico. *Sedimentology*, **37**, 23–43.

Galloway, W.E. (1975) Process framework for describing the morphologic and stratigraphic evolution of deltaic depositional systems.

Geyman, E.C., **Maloof, A.C.** and **Dyer, B.** (2021) How is sea level change encoded in carbonate stratigraphy? *Earth Planet. Sci. Lett.*, **560**, 116790.

Gilbert, G.K. (1877) *Geology of the Henry Mountains*. Government Printing Office, Washington, D.C.

Gilluly, J. (1929) Geology and oil and gas prospects of part of the San Rafael Swell, Utah. *U.S. Geol. Survey Bull.*, **806c**, 69–130.

Goldhammer, R.K., **Dunn, P.A.** and **Hardie, L.A.** (1990) Depositional cycles, composite sea-level changes, cycle stacking patterns, and the hierarchy of stratigraphic forcing: examples from Alpine Triassic platform carbonates. *Geol. Soc. Am. Bull.*, **102**, 535–562.

Gonzalez, R. and **Eberli, G.P.** (1997) Sediment transport and bedforms in a carbonate tidal inlet; Lee Stocking Island, Exumas, Bahamas. *Sedimentology*, **44**, 1015–1030.

Grötsch, J., **Suwaina, O.**, **Ajlani, G.**, **Taher, A.**, **El-Khassawneh, R.**, **Lokier, S.**, **Coy, G.**, **van der Weerd, E.**, **Masalmeh, S.** and **van Dorp, J.** (2003) The Arab Formation in central Abu Dhabi: 3-D reservoir architecture and static and dynamic modeling. *GeoArabia*, **8**, 47–86.

Grotzinger, J.P. (1986) Cyclicity and paleoenvironmental dynamics, Rocknest platform, northwest Canada. *Geol. Soc. Am. Bull.*, **97**, 1208–1231.

Harris, B.S., **Rozanitis, K.J.**, **Sutherland, B.**, **Myers, P.G.**, **Konhauser, K.O.** and **Gingras, M.K.** (2024) Biostabilization: parameterizing the interactions between microorganisms and siliciclastic marine sediments. *Earth-Sci. Rev.*, **259**, 104976.

Hashmie, A., **Rostamnejad, A.**, **Nikbakht, F.**, **Ghorbanie, M.**, **Rezaie, P.** and **Gholamalian, H.** (2016) Depositional environments and sequence stratigraphy of the Bahram Formation (middle–late Devonian) in north of Kerman, south-central Iran. *Geosci. Front.*, **7**, 821–834.

Havholm, K.G. and **Kocurek, G.** (1994) Factors controlling aeolian sequence stratigraphy: clues from super bounding

surface features in the Middle Jurassic Page Sandstone. *Sedimentology*, **41**, 913–934.

Havholm, K.G., **Blakey, R.C.**, **Capps, M.**, **Jones, L.S.**, **King, D.D.** and **Kocurek, G.** (1993) Aeolian genetic stratigraphy: an example from the Middle Jurassic Page Sandstone, Colorado Plateau. In: *Aeolian Sediments: Ancient and Modern* (Eds Pye, K. and Lancaster, N.), 1st edn, pp. 85–107. The International Association of Sedimentologists.

Hintze, L.F., **Willis, G.C.**, **Laes, D.Y.**, **Sprinkel, D.A.** and **Brown, K.D.** (2000) *Digital Geologic Map of Utah*. Utah Geological Survey, Utah.

Hunter, R.E. (1977) Basic types of stratification in small eolian dunes. *Sedimentology*, **24**, 361–387.

Ives, R.L. (1949) Climate of the Sonoran Desert Region. *Ann. Assoc. Am. Geogr.*, **39**, 143–187.

James, N.P. (1984) Shallowing-upward sequences in carbonates. *Facies Models*, **1**, 213–228.

Jones, L.S. and **Blakey, R.C.** (1993) Erosional remnants and adjacent unconformities along an eolian-marine boundary of the Page Sandstone and Carmel Formation, Middle Jurassic, south-central Utah. *J. Sed. Res.*, **63**, 852–859.

Jones, L.S. and **Blakey, R.C.** (1997) Eolian-fluvial interaction in the Page Sandstone (Middle Jurassic) in south-central Utah, USA—a case study of erg-margin processes. *Sed. Geol.*, **109**, 181–198.

Kendall, A.C. (1978) Facies models 11. Continental and supratidal (sabkha) evaporites. *Geosci. Can.*, **5**, 66–78.

Kendall, C.G.S.C. and **Skipwith, P.A.D.** (1969) Holocene shallow-water carbonate and evaporite sediments of Khor al Bazam, Abu Dhabi, southwest Persian Gulf. *AAPG Bull.*, **53**, 841–869.

Kenig, F., **Huc, A.Y.**, **Purser, B.H.** and **Oudin, J.-L.** (1990) Sedimentation, distribution and diagenesis of organic matter in a recent carbonate environment, Abu Dhabi, UAE. *Org. Geochem.*, **16**, 735–747.

Khazaie, E., **Noorian, Y.**, **Kavianpour, M.**, **Moussavi-Harami, R.**, **Mahboubi, A.** and **Omidpour, A.** (2022) Sedimentological and diagenetic impacts on porosity systems and reservoir heterogeneities of the Oligo-Miocene mixed siliciclastic and carbonate Asmari reservoir in the Mansuri oilfield, SW Iran. *J. Pet. Sci. Eng.*, **213**, 110435.

Kinsman, D.J. (1969) Modes of formation, sedimentary associations, and diagnostic features of shallow-water and supratidal evaporites. *AAPG Bull.*, **53**, 830–840.

Kocurek, G. (1981a) Erg reconstruction: the Entrada sandstone (Jurassic) of northern Utah and Colorado. *Palaeogeogr. Palaeoclimatol. Palaeoecol.*, **36**, 125–153.

Kocurek, G. (1981b) Significance of interdune deposits and bounding surfaces in aeolian dune sands. *Sedimentology*, **28**, 753–780.

Kocurek, G. and **Dott, R.H.** (1981) Distinctions and uses of stratification types in the interpretation of eolian sand. *J. Sed. Res.*, **51**, 579–595.

Kocurek, G. and **Dott, R.H.** (1983) Jurassic paleogeography and paleoclimate of the central and southern Rocky Mountains region. *Rocky Mountain Section (SEPM).*

Kocurek, G. and **Hunter, R.E.** (1986) Origin of polygonal fractures in sand, uppermost Navajo and Page Sandstones, Page, Arizona. *J. Sed. Res.*, **56**, 895–904.

Kocurek, G. and **Nielson, J.** (1986) Conditions favourable for the formation of warm-climate aeolian sand sheets. *Sedimentology*, **33**, 795–816.

Kocurek, G., **Robinson, N.I.** and **Sharp, J.M., Jr.** (2001) The response of the water table in coastal aeolian systems to changes in sea level. *Sed. Geol.*, **139**, 1–13.

Koerschner, W.F. and **Read, J.F.** (1989) Field and modelling studies of Cambrian carbonate cycles, Virginia, Appalachians. *J. Sed. Res.*, **59**, 654–687.

Kowallis, B.J., **Christiansen, E.H.**, **Deino, A.L.**, **Zhang, C.** and **Everett, B.H.** (2001) The record of Middle Jurassic volcanism in the Carmel and Temple Cap Formations of southwestern Utah. *GSA Bull.*, **113**, 373–387.

Kowallis, B., **Sprinkel, D.**, **Christiansen, E.**, **Steed, S.** and **Wheatley, D.** (2020) Rhyolite ignimbrite boulders and cobbles in the Middle Jurassic Carmel Formation of Utah and Arizona—age, composition, transport, and stratigraphic setting. *Geol. Intermountain West*, **7**, 69–96.

Kvale, E.P., **Cutright, J.**, **BIlodeau, D.**, **Archer, A.**, **Johnson, H.R.** and **Pickett, B.** (1995) Analysis of modern tides and implications for ancient tidalites. *Cont. Shelf Res.*, **15**, 1921–1943.

Lanier, W.P. and **Tessier, B.** (1998) Climbing-ripple bedding in the fluvio-estuarine transition: a common feature associated with tidal dynamics (modern and ancient analogues).

Lasemi, Y., **Jahani, D.**, **Amin-Rasouli, H.** and **Lasemi, Z.** (2012) Ancient Carbonate Tidalites. In: *Principles of Tidal Sedimentology* (Eds Davis, R.A. and Dalrymple, R.W.), pp. 567–607. Springer Netherlands, Dordrecht.

Lokier, S.W. (2012) Development and evolution of subaerial halite crust morphologies in a coastal sabkha setting. *J. Arid Environ.*, **79**, 32–47.

Lokier, S.W. and **Fiorini, F.** (2016) Temporal evolution of a carbonate coastal system, Abu Dhabi, United Arab Emirates. *Mar. Geol.*, **381**, 102–113.

Lokier, S. and **Steuber, T.** (2008) Quantification of carbonate-ramp sedimentation and progradation rates for the late Holocene Abu Dhabi shoreline. *J. Sed. Res.*, **78**, 423–431.

Lokier, S.W., **Knaf, A.** and **Kimiagar, S.** (2013) A quantitative analysis of Recent arid coastal sedimentary facies from the Arabian Gulf Coastline of Abu Dhabi, United Arab Emirates. *Mar. Geol.*, **346**, 141–152.

Longhitano, S.G. (2011) The record of tidal cycles in mixed silici–bioclastic deposits: examples from small Plio–Pleistocene peripheral basins of the microtidal Central Mediterranean Sea. *Sedimentology*, **58**, 691–719.

Longhitano, S.G. and **Miocic, J.M.** (2024) The regressive surface of marine erosion generated by tides: a case study from a Pleistocene tidal sand ridge sequence, Calabria, Southern Italy. *Depos. Rec.*, **11**, dep2.300.

Longhitano, S.G., **Sabato, L.**, **Tropeano, M.** and **Gallicchio, S.** (2010) A mixed bioclastic-siliciclastic flood-tidal delta in a micro tidal setting: depositional architectures and hierarchical internal organization (Pliocene, Southern Apennine, Italy). *J. Sed. Res.*, **80**, 36–53.

Longhitano, S.G., **Chiarella, D.**, **Di Stefano, A.**, **Messina, C.**, **Sabato, L.** and **Tropeano, M.** (2012a) Tidal signatures in Neogene to Quaternary mixed deposits of southern Italy straits and bays. *Sed. Geol.*, **279**, 74–96.

Longhitano, S.G., **Mellere, D.**, **Steel, R.J.** and **Ainsworth, R.B.** (2012b) Tidal depositional systems in the rock record: a review and new insights. *Sed. Geol.*, **279**, 2–22.

Longhitano, S.G., **Chiarella, D.** and **Muto, F.** (2014) Three-dimensional to two-dimensional cross-strata transition in the lower Pleistocene Catanzaro tidal strait transgressive succession (southern Italy). *Sedimentology*, **61**, 2136–2171.

Lucas, S.G. and **Anderson, O.J.** (1997) The Jurassic San Rafael Group, Four Corners region. *Mesozoic Geology and Paleontology of the Four Corners Region: New Mexico*

Geological Society, 48th Annual Fall Field Conference Guidebook, The New Mexico Geological Society USA, 115–132.

Manifold, L., **Hollis, C.** and **Burgess, P.** (2020) The Anatomy of a Mississippian (Viséan) carbonate platform interior, UK: depositional cycles, glacioeustasy and facies mosaics. *Sed. Geol.*, **401**, 105633.

Marzolf, J.E. (1991) Lower Jurassic unconformity (J-0) from the Colorado Plateau to the eastern Mojave Desert: evidence of a major tectonic event at the close of the Triassic. *Geology*, **19**, 320–323.

McCubbin, D.G. (1982) Barrier-Island and Strand-Plain Facies.

Melnyk, S., **Lazowski, C.N.**, **Dashtgard, S.E.** and **Gingras, M.K.** (2025) Topographic controls on the distribution of bioturbation in an intertidal sandflat. *Sedimentology*, **72**, 613–630.

Mountney, N.P. (2006) Periodic accumulation and destruction of aeolian erg sequences in the Permian Cedar Mesa Sandstone, White Canyon, southern Utah, USA. *Sedimentology*, **53**, 789–823.

Mountney, N.P. and **Thompson, D.B.** (2002) Stratigraphic evolution and preservation of aeolian dune and damp/wet interdune strata: an example from the Triassic Helsby Sandstone Formation, Cheshire Basin, UK. *Sedimentology*, **49**, 805–833.

Musial, G., **Reynaud, J.-Y.**, **Gingras, M.K.**, **Féniès, H.**, **Labourdette, R.** and **Parize, O.** (2012) Subsurface and outcrop characterization of large tidally influenced point bars of the Cretaceous McMurray Formation (Alberta, Canada). *Sed. Geol.*, **279**, 156–172.

Myrow, P.M. and **Southard, J.B.** (1996) Tempestite deposition. *J. Sed. Res.*, **66**, 875–887.

Olariu, C., **Steel, R.J.**, **Dalrymple, R.W.** and **Gingras, M.K.** (2012) Tidal dunes versus tidal bars: the sedimentological and architectural characteristics of compound dunes in a tidal seaway, the lower Baronia Sandstone (Lower Eocene), Ager Basin, Spain. *Sed. Geol.*, **279**, 134–155.

Osleger, D. (1991) Subtidal carbonate cycles: implications for allocyclic vs. autocyclic controls. *Geology*, **19**, 917–920.

Parrish, J.T. and **Peterson, F.** (1988) Wind directions predicted from global circulation models and wind directions determined from eolian sandstones of the western United States—A comparison. *Sed. Geol.*, **56**, 261–282.

Paul, A., **Lokier, S.W.**, **Sherry, A.**, **Andrade, L.L.**, **Court, W.M.**, **Van Der Land, C.**, **Dutton, K.E.** and **Head, I.M.** (2021) Erosion-initiated stromatolite and thrombolite formation in a present-day coastal sabkha setting. *Sedimentology*, **68**, 382–401.

Peel, M.C., **Finlayson, B.L.** and **McMahon, T.A.** (2007) Updated world map of the Köppen-Geiger climate classification. *Hydrol. Earth Syst. Sci.*, **11**, 1633–1644.

Peterson, F. and **Pipiringos, G.N.** (1979) *Stratigraphic relations of the Navajo Sandstone to Middle Jurassic formations, southern Utah and northern Arizona*. US Geological Survey, Reston, VA.

Pettigrew, R.P., **Priddy, C.**, **Clarke, S.M.**, **Warke, M.R.**, **Stüeken, E.E.** and **Claire, M.W.** (2021) Sedimentology and isotope geochemistry of transitional evaporitic environments within arid continental settings: from erg to saline lakes. *Sedimentology*, **68**, 907–942.

Picard, M.D. and **Uygur, K.** (1982) Mixed terrigenous-carbonate rocks in Jurassic Arapien Shale of central Utah. *Utah Geol. Assoc. Publ.*, **10**, 181–198.

Pipiringos, G.N. and **O'Sullivan, R.B.** (1978) *Principal unconformities in Triassic and Jurassic rocks, western interior United States-a preliminary survey*. United States Government Printing Office, Washington, DC.

Pratt, B. (2010) Peritidal carbonates. In: *Facies Models 4* (Eds James, N.P. and Dalrymple, R.G.). Geological Association of Canada, St. John's, Canada.

Pratt, B.R. and **James, N.P.** (1986) The St George Group (Lower Ordovician) of western Newfoundland: tidal flat Island model for carbonate sedimentation in shallow epeiric seas. *Sedimentology*, **33**, 313–343.

Priddy, C.L., **Pettigrew, R.P.**, **Watson, D.**, **Regis, A.V.** and **Clarke, S.M.** (2023) Aeolian–lacustrine margins: implications for carbon capture and storage within the Rotliegend Group, Southern North Sea. *Geoenergy*, geoenergy2023-031.

Qiao, Z., **Janson, X.**, **Shen, A.**, **Zheng, J.**, **Zeng, H.** and **Wang, X.** (2016) Lithofacies, architecture, and reservoir heterogeneity of tidal-dominated platform marginal oolitic shoal: an analogue of oolitic reservoirs of Lower Triassic Feixianguan Formation, Sichuan Basin, SW China. *Mar. Petrol. Geol.*, **76**, 290–309.

Quijada, I.E., **Suarez-Gonzalez, P.**, **Benito, M.I.** and **Mas, R.** (2016) Tidal versus continental sandy-muddy flat deposits. In: *Contributions to Modern and Ancient Tidal Sedimentology* (Eds Tessier, B. and Reynaud, J.Y.), pp. 133–159. John Wiley & Sons, Ltd, Oxford, UK.

Quijada, I.E., **Benito, M.I.**, **Suarez-Gonzalez, P.**, **Rodríguez-Martínez, M.** and **Campos-Soto, S.** (2020) Challenges to carbonate-evaporite peritidal facies models and cycles: insights from Lower Cretaceous stromatolite-bearing deposits (Oncala Group, N Spain). *Sed. Geol.*, **408**, 105752.

Rankey, E.C. (2016) On facies belts and facies mosaics: Holocene isolated platforms, South China Sea. *Sedimentology*, **63**, 2190–2216.

Rankey, E.C. and **Reeder, S.L.** (2012) Tidal Sands of the Bahamian Archipelago. In: *Principles of Tidal Sedimentology* (Eds Davis, R.A. and Dalrymple, R.W.), pp. 537–565. Springer Netherlands, Dordrecht.

Read, J.F., **Markello, J.R.**, **Koerschner, W.F.**, **Sundberg, F.A.** and **Osleger, D.A.** (2025) Orbitally forced aquifer eustasy controlled cycle- and ~1.3 Myr sequence development: middle to basal Upper Cambrian coeval rift and continental shelf facies, eastern USA. *Palaeogeogr. Palaeoclimatol. Palaeoecol.*, **662**, 112716.

Reineck, H. and **Wunderlich, F.** (1968) Classiffication and origin of flaser and lenticular bedding. *Sedimentology*, **11**, 99–104.

Riding, R. and **Wright, V.P.** (1981) Paleosols and tidal-flat/lagoon sequences on a Carboniferous carbonate shelf; sedimentary associations of triple disconformities. *J. Sed. Res.*, **51**, 1323–1339.

Rivers, J.M. and **Dalrymple, R.W.** (2025) Facies stacking patterns in modern carbonate peritidal settings and their sequence-stratigraphic implications. *Earth-Sci. Rev.*, **269**, 105201.

Rivers, J.M., **Dalrymple, R.W.**, **Yousif, R.**, **Al-Shaikh, I.**, **Butler, J.D.**, **Warren, C.**, **Skeat, S.L.** and **Bari, E.M.A.** (2020) Mixed siliciclastic-carbonate-evaporite sedimentation in an arid eolian landscape: the Khor Al Adaid tide-dominated coastal embayment, Qatar. *Sed. Geol.*, **408**, 105730.

Rodrigues, M.G., **Giovanini Varejão, F.**, **Fürsich, F.T.**, **Christofoletti, B.**, **Matos, S.A.**, **Warren, L.V.**, **Inglez, L.**,

Cerri, R.I., **Assine, M.L.** and **Simões, M.G.** (2024) Not all shell beds are made equal: recognizing singular event-concentrations in megalakes. *Sedimentology*, **71**, sed.13221.

Rodríguez-López, J.P., **Meléndez, N.**, **De Boer, P.L.** and **Soria, A.R.** (2012) Controls on marine–erg margin cycle variability: aeolian–marine interaction in the mid-Cretaceous Iberian Desert System, Spain. *Sedimentology*, **59**, 466–501.

Rubin, D.M. and **Hunter, R.E.** (1982) Bedform climbing in theory and nature. *Sedimentology*, **29**, 121–138.

Sarkar, S., **Choudhuri, A.**, **Mandal, S.** and **Eriksson, P.G.** (2016) Microbial mat-related structures shared by both siliciclastic and carbonate formations. *J. Palaeogeogr.*, **5**, 278–291.

Scheidt, S., **Lancaster, N.** and **Ramsey, M.** (2011) Eolian dynamics and sediment mixing in the Gran Desierto, Mexico, determined from thermal infrared spectroscopy and remote-sensing data. *Bulletin*, **123**, 1628–1644.

Sequero, C., **Bádenas, B.** and **Aurell, M.** (2018) Facies mosaic in the inner areas of a shallow carbonate ramp (Upper Jurassic, Higueruelas Fm, NE Spain). *Facies*, **64**, 9.

Shinn, E.A. (1983) Birdseyes, fenestrae, shrinkage pores, and loferites; a reevaluation. *J. Sed. Res.*, **53**, 619–628.

Sleveland, A.R., **Midtkandal, I.**, **Galland, O.** and **Leanza, H.A.** (2020) Sedimentary architecture of storm-influenced tidal flat deposits of the upper Mulichinco Formation, Neuquén Basin, Argentina. *Front. Earth Sci.*, **8**, 219.

Smyrak-Sikora, A., **Osmundsen, P.T.**, **Braathen, A.**, **Ogata, K.**, **Anell, I.**, **Mulrooney, M.J.** and **Zuchuat, V.** (2020) Architecture of growth basins in a tidally influenced, prodelta to delta-front setting: the Triassic succession of Kvalpynten, East Svalbard. *Basin Res.*, **32**, 949–978.

Spalluto, L. (2008) Sedimentology and high-resolution sequence stratigraphy of a lower Cretaceous shallow-water carbonate succession from the Western Gargano Promontory (Apulia, Southern Italy). *Geoacta Spec. Publ.*, **1**, 173–192.

Spalluto, L., **Petruzzelli, M.**, **Sabato, L.** and **Tropeano, M.** (2024) Cretaceous cyclic peritidal carbonates of the Apulia Carbonate Platform (Apulia, southern Italy) in a hierarchical sequence-stratigraphic perspective: a case study from the Murge area (the Giovinazzo sea-cliff section). *Depos. Rec.*, **11**, dep2.305.

Sprinkel, D.A. (1982) Twin Creek Limestone-Arapien Shale relations in central Utah.

Sprinkel, D.A., **Doelling, H.H.**, **Kowallis, B.J.**, **Waanders, G.**, **Kuehne, P.A.**, **Yonkee, W.A.** and **Chidsey, T.C.** (2011) Early results of a study of Middle Jurassic strata in the Sevier fold and thrust belt, Utah. In: *Sevier Thrust Belt: northern and Central Utah and Adjacent Areas*, Vol. **40**, pp. 151–172. Utah Geological Association Publication, Utah.

Sprinkel, D., **Doelling, H.H.**, **Kowallis, B.J.**, **Waanders, G.** and **Kuehne, P.A.** (2024) Stratigraphy, correlation, and age of the Gypsum Spring, Temple Cap, Arapien, Carmel, and Twin Creek Formations (Early and Middle Jurassic) of Utah and surrounding states. *Utah Geol. Surv. Contract Deliverable*, **18**, 220.

Steel, R.J., **Plink-Bjorklund, P.** and **Aschoff, J.** (2012) Tidal deposits of the Campanian Western Interior Seaway, Wyoming, Utah and Colorado, USA. In: *Principles of Tidal Sedimentology* (Eds Davis, R.A. and Dalrymple, R.W.), pp. 437–471. Springer Netherlands, Dordrecht.

Suarez-Gonzalez, P., **Benito, M.I.**, **Quijada, I.E.**, **Mas, R.** and **Campos-Soto, S.** (2019) 'Trapping and binding': a review of the factors controlling the development of fossil agglutinated microbialites and their distribution in space and time. *Earth-Sci. Rev.*, **194**, 182–215.

Tang, C.M., **Bottjer, D.J.** and **Simms, M.J.** (2000) Stalked crinoids from a Jurassic tidal deposit in western North America. *Lethaia*, **33**, 46–54.

Taylor, P.D. and **Wilson, M.A.** (1999) Middle Jurassic bryozoans from the Carmel Formation of southwestern Utah. *J. Paleontol.*, **73**, 816–830.

Tessier, B. and **Gigot, P.** (1989) A vertical record of different tidal cyclicities: an example from the Miocene Marine Molasse of Digne (Haute Provence, France). *Sedimentology*, **36**, 767–776.

Thorman, C.H. (2011) The Elko orogeny–A major tectonic event in eastern Nevada–western Utah. In: *Sevier Thrust Belt: northern and Central Utah and Adjacent Areas* (Eds Sprinkel, D.A., Yonkee, W.A. and Chidsey, T.C., Jr.), Vol. **40**, pp. 117–129. Utah Geological Association Publication, Utah.

Vakarelov, B.K., **Ainsworth, R.B.** and **MacEachern, J.A.** (2012) Recognition of wave-dominated, tide-influenced shoreline systems in the rock record: variations from a microtidal shoreline model. *Sed. Geol.*, **279**, 23–41.

Védrine, S., **Strasser, A.** and **Hug, W.** (2007) Oncoid growth and distribution controlled by sea-level fluctuations and climate (Late Oxfordian, Swiss Jura Mountains). *Facies*, **53**, 535–552.

Visser, M.J. (1980) Neap-spring cycles reflected in Holocene subtidal large-scale bedform deposits: a preliminary note. *Geology*, **8**, 543–546.

Wheatley, D.F. and **Chan, M.A.** (2018) Clastic pipes and soft-sediment deformation of the Jurassic Carmel Formation, southern Utah, USA: implications for pipe formation mechanisms and host-rock controls. *J. Sed. Res.*, **88**, 1076–1095.

Wilkinson, B.H., **Diedrich, N.W.** and **Drummond, C.N.** (1996) Facies successions in peritidal carbonate sequences. *J. Sed. Res.*, **66**, 1065–1078.

Wilkinson, B.H., **Drummond, C.N.**, **Rothman, E.D.** and **Diedrich, N.W.** (1997) Stratal order in peritidal carbonate sequences. *J. Sed. Res.*, **67**, 1068–1082.

Wilson, K. and **Mohrig, D.** (2021) Modern coastal tempestite deposition by a non-local storm: swell-generated transport of sand and boulders on Eleuthera, The Bahamas. *Sedimentology*, **68**, 2043–2068.

Wilson, M.A. and **Palmer, T.J.** (1994) A carbonate hardground in the Carmel Formation (Middle Jurassic, SW Utah, USA) and its associated encrusters, borers and nestlers. *Ichnos*, **3**, 79–87.

Wilson, M.A., **Ozanne, C.R.** and **Palmer, T.J.** (1998) Origin and paleoecology of free-rolling oyster accumulations (ostreoliths) in the Middle Jurassic of southwestern Utah, USA. *Palaios*, **13**, 70–78.

Wood, G.V. and **Wolfe, M.J.** (1969) Sabkha cycles in the Arab/Darb Formation off the Trucial coast of Arabia. *Sedimentology*, **12**, 165–191.

Wroblewski, A.F.-J. and **Morris, E.A.** (2023) Unconformity generation and the shift from storm-dominated to tide-dominated processes in a Jurassic retroarc foreland basin: insights from ichnology. *Depos. Rec.*, **9**, 253–299.

Wroblewski, A.F.-J. and **Schueth, J.** (2023) Subtidal to intertidal deposits in a mixed clastic–carbonate epicontinental seaway, the Windy Hill Sandstone and Upper Sundance Formation (Oxfordian), Wyoming, USA. *J. Sed. Res.*, **93**, 571–594.

Wroblewski, A.F.-J., **Steel, R.J.**, **Morris, E.A.** and **Schueth, J.** (2024) A tale of two end members: tidal deposits in a semi-arid, low subsidence, open coastal setting versus a high runoff, high subsidence, restricted environment. *Depos. Rec.*, **10**, dep2.284.

Yoshida, S., **Jackson, M.D.**, **Johnson, H.D.**, **Muggeridge, A.H.** and **Martinius, A.W.** (2001) *Outcrop Studies of Tidal Sandstones for Reservoir Characterization (Lower Cretaceous Vectis Formation, Isle of Wight, Southern England)*, Vol. **10**, pp. 233–257. Norwegian Petroleum Society Special Publications, Elsevier.

Yoshida, S., **Steel, R.J.** and **Dalrymple, R.W.** (2007) Changes in depositional processes—an ingredient in a new generation of sequence-stratigraphic models. *J. Sed. Res.*, **77**, 447–460.

Zhong, Y., **Lokier, S.W.**, **Pederson, C.L.**, **Fiorini, F.**, **Hennhoefer, D.**, **Ge, Y.** and **Immenhauser, A.** (2023) Carbonate sediment dynamics in the Abu Dhabi lagoon-implications for low-angle inner-to-middle ramp models. *Mar. Geol.*, **465**, 107172.

Zuchuat, V., **Sleveland, A.**, **Sprinkel, D.**, **Rimkus, A.**, **Braathen, A.** and **Midtkandal, I.** (2018) New insights on the impact of tidal currents on a low-gradient, semi-enclosed, epicontinental basin—the Curtis Formation, east-central Utah, USA. *Geol. Intermountain West*, **5**, 131–165.

Zuchuat, V., **Sleveland, A.R.N.**, **Pettigrew, R.P.**, **Dodd, T.J.H.**, **Clarke, S.M.**, **Rabbel, O.**, **Braathen, A.** and **Midtkandal, I.** (2019) Overprinted allocyclic processes by tidal resonance in an epicontinental basin: the Upper Jurassic Curtis Formation, east-central Utah, USA. *Depos. Rec.*, **5**, 272–305.

Zuchuat, V., **Steel, E.**, **Mulligan, R.P.**, **Collins, D.S.** and **Green, J.A.M.** (2022) Tidal dynamics in palaeo-seas in response to changes in physiography, tidal forcing and bed shear stress. *Sedimentology*, **69**, 1861–1890.

Zuchuat, V., **Gugliotta, M.**, **Poyatos-Moré, M.**, **van der Vegt, H.**, **Collins, D.S.** and **Vaucher, R.** (2023) Mixed depositional processes in coastal to shelf environments: towards acknowledging their complexity. *Depos. Rec.*, **9**, 206–212.

Manuscript received 17 March 2025; revision accepted 12 September 2025